第 44 卷 第 4 期 地 质 通 报 Vol. 44, No.4
2025 年 4 月 GEOLOGICAL BULLETIN OF CHINA Apr., 2025

doi: 10.12097/gbc.2024.12.011

原特提斯和古特提斯碰撞岩浆与斑岩成矿：以东昆仑祁漫塔格地区为例

钟世华[1,2]，李三忠[1,2]，丰成友[3]，汤贺军[4]，张勇[5]，何书跃[5]

ZHONG Shihua[1,2], LI Sanzhong[1,2], FENG Chengyou[3], TANG Hejun[4], ZHANG Yong[5], HE Shuyue[5]

1. 中国海洋大学海洋地球科学学院/海底科学与探测技术教育部重点实验室, 山东 青岛 266100;
2. 青岛海洋科技中心海洋矿产资源评价与探测技术功能实验室, 山东 青岛 266237;
3. 中国地质调查局, 北京 100037;
4. 中国地质科学院, 北京 100037;
5. 青海省第三地质勘查院, 青海 西宁 810029

1. *College of Marine Geosciences/Key Lab of Submarine Geosciences and Prospecting Techniques, MOE and Ocean University of China, Qingdao* 266100, *Shandong, China;*
2. *Laboratory for Marine Mineral Resources, Qingdao Marine Science and Technology Center, Qingdao* 266237, *Shandong, China;*
3. *China Geology Survey, Beijing* 100037, *China;*
4. *Chinese Academy of Gelogical Sciences, Beijing* 100037, *China;*
5. *The Third Geological Exploration Institute of Qinghai Province, Xining* 810029, *Qinghai, China*

摘要:【研究目的】特提斯分为原特提斯、古特提斯和新特提斯，分别大致对应于早古生代、晚古生代和中生代期间的大洋。研究表明，新特提斯洋闭合后形成的（后）碰撞花岗岩类普遍具有高氧逸度和富水的特征，使这些地区形成了许多大型—超大型斑岩铜矿。然而，关于原特提斯和古特提斯斑岩铜矿的成矿潜力，特别是这 2 个古大洋闭合后的（后）碰撞阶段是否具备类似潜力，尚未进行系统研究。东昆仑祁漫塔格地区记录了原、古特提斯从俯冲到闭合阶段的构造演化和成矿历史，成为研究原特提斯和古特提斯斑岩成矿作用的天然实验室和绝佳场所。**【研究方法】**本文综述了东昆仑祁漫塔格地区以往报道的花岗岩类年龄和地球化学资料，着重讨论了与斑岩-矽卡岩矿床有关的花岗岩类特征，揭示原特提斯和古特提斯斑岩成矿规律，服务新一轮找矿突破战略行动。**【研究结果】**东昆仑祁漫塔格地区花岗岩类主要集中出现于 2 个时期，即 435~370 Ma 和 245~196 Ma，分别形成于原特提斯洋和古特提斯洋闭合后的碰撞阶段，而与大洋俯冲有关的花岗岩类出露很少。2 期碰撞花岗岩类具有类似的地球化学特征，主要落入高钾钙碱性和钾玄岩系列范围内，属于偏铝质—弱过铝质岩石，亏损 Na 和 Ta，岩浆源区表现出壳幔混合特征。**【结论】**综合前人研究成果，提出原、古特提斯洋经历了类似的演化过程：①俯冲阶段，原、古特提斯洋壳均以平板俯冲的形式向陆块俯冲，抑制了弧岩浆作用，导致东昆仑祁漫塔格地区弧花岗岩类不发育；②碰撞阶段，俯冲板片裂离导致软流圈上涌，形成了大规模的壳幔混合成因的碰撞花岗岩类。与新特提斯碰撞花岗岩类相比，原特提斯和古特提斯碰撞花岗岩类普遍具有较低的氧逸度和水含量。这些特征可以解释为何青藏高原北部没有发现大型—超大型斑岩铜矿床。尽管如此，青藏高原北部矽卡岩铜多金属矿床找矿潜力巨大，应该作为未来找矿的主攻类型和方向。

关键词: 原特提斯；古特提斯；斑岩系统；青海；祁漫塔格

创新点: 青藏高原北部的原、古特提斯洋经历了类似的演化过程，原特提斯和古特提斯碰撞花岗岩类具有较低的氧逸度和水含量，不利于大型斑岩铜矿的形成，矽卡岩矿床应作为该地区找矿的主攻类型。

中图分类号: P618.2; P618.41 **文献标志码:** A **文章编号:** 1671−2552(2025)04−0511−23

收稿日期: 2024−12−03; **修订日期:** 2025−01−02

资助项目: 国家自然科学基金项目《青海野马泉矿床成矿岩浆 H_2O 和 Cl 含量精细研究: 对矽卡岩矿床成因的约束》(批准号: 42203066)、《基于多维数据的斑岩 Cu 矿床成矿岩浆机器学习识别方法和矿床成因研究》(批准号: 42472104)和青海省科技厅项目《青海省祁漫塔格地区铜镍钴找矿突破研究》(编号: 2024028ky002)

作者简介: 钟世华(1989−)，男，博士，副教授，从事矿床学研究。E−mail: zhongshihua@ouc.edu.cn

Zhong S H, Li S Z, Feng C Y, Tang H J, Zhang Y, He S Y. Proto-Tethys and Paleo-Tethys collisional magmas and porphyry mineralization: A case study of the Qimantagh area, East Kunlun Mountains. *Geological Bulletin of China*, 2025, 44(4): 511−533

Abstract: [Objective] Tethys can be divided into Proto−Tethys, Paleo−Tethys and Neo−Tethys according to its evolutionary history, roughly corresponding to the Early Paleozoic, Late Paleozoic and Mesozoic oceans, respectively. In recent years, a large number of studies in the southern Tibetan Plateau, Iran, Pakistan and other areas have shown that the (post−) collisional granite formed after the closure of the New Tethys Ocean is generally characterized by high oxygen fugacity and high water contents, which has led to the formation of many large to super−large porphyry copper deposits in these areas. How about the metallogenic potential of Proto−Tethys and Paleo−Tethys porphyry deposits? Does the (post−) collisional stage after the closure of the two paleo−oceans also have the metallogenic potential of large to super−large porphyry copper deposits? These problems have not been systematically studied before. The Qimantagh area in the East Kunlun Orogenic Belt records the tectonic evolution and metallogenic history of Proto− and Paleo−Tethys from subduction to closed stages. Thus, this area is a natural laboratory and excellent place to study the porphyry mineralization of Proto−Tethys and Paleo−Tethys. **[Methods]** In this paper, the age and geochemical data of granites previously reported in Qimantagh area of the East Kunlun Orogenic Belt are reviewed, and the granite characteristics related to porphyrie−skarn deposits are particularly studied. The purpose of this paper is to reveal the metallogenic regularity of Proto−Tethys and Paleo−Tethys porphyry and serve a new round of prospecting breakthrough strategy. **[Results]** The granites in the Qimantagh area of the East Kunlun Orogenic Belt mainly occurred in two periods, i.e., 435~370 Ma and 245~196 Ma. These granites formed in the collisional stage after the closing of the Proto−Tethys and the Paleo−Tethys Oceans, respectively. In contrast, the granites related to oceanic subduction were rarely found. The two stage collisional granites have similar geochemical characteristics, mainly fall into the range of high−K calc−alkaline and shoshonitic series, belong to metaluminous to weakly peraluminous rocks with depleted Nb and Ta, and display characterisitics of crustal−mantle mixing in the sources of parental magmas. **[Conclusions]** Based on the results of previous studies, this paper proposes that the Proto−Tethys and Paleo−Tethys experienced similar evolutionary processes. ① During the subduction stage, the Proto−Tethys and Paleo−Tethys subducted to the continent in the form of flat subduction, which inhibited arc magmatism and resulted in the scarcity of arc granites in Qimantagh area, East Kunlun. ② During the collisional stage, the subduction plate was detached which led to the upwelling of the asthenosphere mantle, forming a large number of collisional granites of crustal−mantle mixing origin. However, compared with the Neo−Tethys collisional granites, the Proto−Tethys and Paleo−Tethys collisional granites generally have lower oxygen fugacity and water content. These characteristics may explain why no large and super−large porphyry copper deposits have been found in the northern part of the Tibetan Plateau. In spite of this, the skarn copper polymetallic deposits in the north of the Qinghai−Tibet Plateau have great prospecting potential and should be the main type and direction of prospecting in the future.

Key words: Proto-Tethys; Paleo-Tethys; porphyry system; Qinghai; Qimantagh

Highlights: The Proto-Tethys Ocean and Paleo-Tethys Ocean in northern Tibetan Plateau underwent similar evolutionary processes. The collision-related granitoids associated with both Proto-Tethys and Paleo-Tethys exhibit relatively low oxygen fugacity and water content, which are unfavorable for the formation of large porphyry copper deposits. Therefore, skarn-type deposits should be considered as the primary target for mineral exploration in this region.

特提斯成矿域横亘于地球中纬度地区，主体是现今地球表面最雄伟壮观的陆-陆碰撞造山带，西起地中海西部，向东沿阿尔卑斯穿越土耳其-伊朗高原、巴基斯坦、阿富汗、帕米尔地区至喜马拉雅-青藏高原，之后转入中南半岛，终结于印尼苏门答腊群岛，延伸超过 12000 km，是全球三大成矿域之一 (王瑞等, 2020; 吴福元等, 2020; 朱日祥等, 2022; 丁林, 2024)。特提斯成矿域的形成与显生宙时期位于北方劳亚大陆和南方冈瓦纳大陆之间的巨型海洋演变密切相关。根据这一巨型海洋的演化历史，前人将其进一步划分为原特提斯洋(Proto-Tethys Ocean)、古特提斯洋(Paleo-Tethys Ocean)和新特提斯洋(Neo-Tethys Ocean)，分别大致对应于早古生代、晚古生代和中生代期间的大洋 (李三忠等, 2016a; 王瑞等, 2020; 吴福元等, 2020)。原特提斯洋、古特提斯洋和新特提斯洋均消失在特提斯构造域(图 1)，这些古大

洋在不同时期的演化和最终闭合造就了特提斯成矿域复杂的地球动力学特征和优越的成矿条件 (Hou et al., 2012;唐菊兴, 2019; 吕鹏瑞等, 2020; Yu et al., 2021; 李忠海等, 2023; 张安顺等, 2023; 李文渊, 2024)。

进入 21 世纪以来, 对特提斯成矿域构造演化和成矿规律研究取得了重大进展, 先后发现大量的斑岩-矽卡岩铜多金属矿床, 如雄村斑岩铜金矿集区、玉龙铜矿、驱龙铜矿等 (侯增谦等, 2007; 侯增谦, 2010; 唐菊兴等, 2012; 唐菊兴, 2019; 王瑞等, 2020)。在中国境内, 特提斯成矿域出露的大型—超大型斑岩-矽卡岩铜多金属矿床集中出现于青藏高原南部, 并且这些矿床大都与新特提斯洋的演化密切相关, 尤其是在新特提斯洋闭合后的后碰撞阶段爆发 (唐菊兴等, 2012; 王瑞等, 2020)。相比于新特提斯洋, 青藏高原南部尚未发现与原特提斯洋演化有关的斑岩-矽卡岩矿床, 而与古特提斯洋有关的斑岩成矿系统也鲜有报道 (Richards and Şengör, 2017)。因此, 国内外对特提斯成矿域斑岩成矿作用的研究高度聚焦于新特提斯, 而很少关注原特提斯和古特提斯。Richards and Şengör (2017) 通过汇编全球数据指出, 古特提斯弧岩浆比新特提斯弧岩浆氧逸度低, 抑制了斑岩铜矿的成矿潜力, 但该研究没有涉及原特提斯, 也没有对比 3 个古大洋闭合后的碰撞阶段岩浆成矿能力。3 个古大洋的地球动力学演化和成矿规律是否具有本质上的差异? 特别是, 原特提斯和古特提斯 2 个古大洋闭合后形成的碰撞岩浆是否本身不利于大型斑岩-矽卡岩矿床的形成? 目前对这些关键问题的研究仍处于空白, 严重制约了对特提斯成矿域形成演化规律和资源环境效应的全面认识。

东昆仑祁漫塔格地区位于青藏高原北部, 是中国西北地区重要的斑岩-矽卡岩型铜铁多金属成矿带 (丰成友等, 2010; 高永宝, 2013; 于淼等, 2017; 郭广慧等, 2023;何书跃等, 2023; 刘嘉情等, 2023)。与青藏高原南部不同, 该地区原特提斯和古特提斯地质记录十分丰富, 出露大量的早古生代—中生代岩浆岩 (瞿泓滢等, 2018; 王秉璋等, 2021; Deng et al., 2024), 记录了原、古特提斯洋从俯冲到闭合阶段的构造演化和成矿历史 (于淼等, 2017), 成为研究原特提斯和古特提斯斑岩成矿作用的天然实验室和绝佳场所 (钟世华, 2018; Zhong et al., 2021b; Dong et al., 2024)。本文在简要回顾东昆仑原、古特提斯洋构造

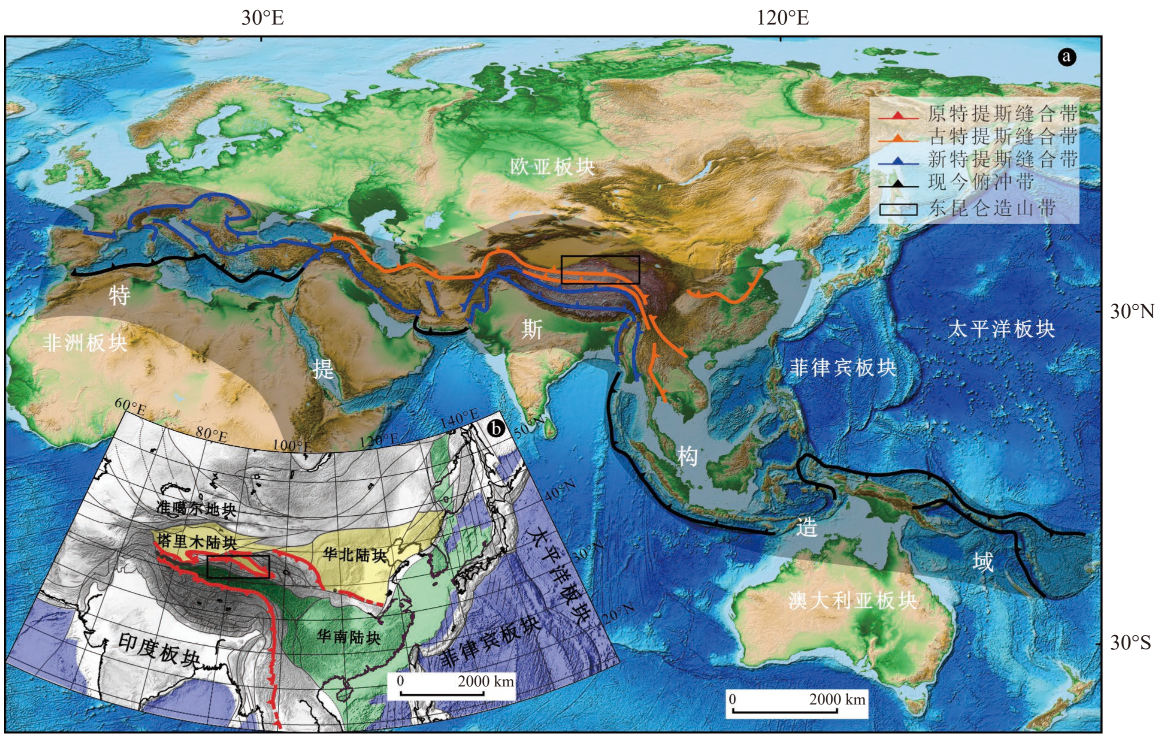

图 1　特提斯构造域古特提斯和新特提斯缝合带位置 (a, 据吴福元等, 2020; 朱日祥等, 2022 修改) 和东亚原特提斯缝合带位置 (b, 据 Li et al., 2018b 修改)

Fig. 1　Locations of Paleo- and Neo-Tethys sutures in the Tethys tectonic domain (a) and Proto-Tethys sutures in East Asia (b)

演化历史的基础上,着重讨论了与斑岩-矽卡岩铜多金属矿床有关的 2 期碰撞花岗岩类的岩相学和地球化学特征,并与新特提斯造山作用形成的大型—超大型碰撞斑岩成矿系统进行对比,以期揭示原特提斯和古特提斯斑岩成矿规律,服务新一轮找矿突破战略行动。

1 特提斯演化概述

特提斯(Tethys),又名特提斯洋或特提斯海,最初由奥地利地质学家 Eduard Suess 于 1893 年提出,用来描述北方安加拉大陆(Angara)与南方冈瓦纳大陆之间的海洋,名字来源于希腊神话中女神特提斯(Tethys)。不同时期的特提斯洋及周缘存在许多微陆块和微洋块 (Li et al., 2018a),这使得特提斯构造域在演化过程中经历了复杂的洋-陆俯冲和聚散过程,也导致原特提斯、古特提斯和新特提斯边界、俯冲极性、打开和闭合时限等许多问题仍存在不同的观点 (Metcalfe, 2013; Deng et al., 2014; 李三忠等, 2016b; Li et al., 2018b; 吴福元等, 2020; Yu et al., 2021;朱日祥等, 2022; Dong et al., 2024;丁林, 2024;傅恒等, 2024; 李文渊, 2024; 辛仁臣, 2024)。

目前的主流观点认为,原特提斯洋是位于北美劳伦-波罗的海-塔里木-华北和冈瓦纳大陆之间,由 Rodinia 超大陆裂解而来的大洋 (吴福元等, 2020),在 480~400 Ma,伴随着扬子、塔里木、柴达木等一系列(微)陆块南向俯冲至冈瓦纳大陆北缘,原特提斯洋发生闭合 (Li et al., 2018b)。古特提斯洋何时开裂存在明显的争论,如 Li et al. (2018b) 认为,在 380 Ma 华南陆块和塔里木-华北陆块从冈瓦纳大陆北缘的裂离导致了古特提斯洋的形成,而李文渊 (2024) 认为与古特提斯洋形成有关的陆块裂解可能在志留纪就开始发生(440~420 Ma)。古特提斯洋的闭合大致发生在中—晚三叠世,形成华夏复合块体,并导致全球意义上 Pangea 超大陆的形成 (吴福元等, 2020)。新特提斯洋的扩张开始于早三叠世 (吴福元等, 2020),或甚至更早 (Şengör, 1979; 朱日祥等, 2022),此时古特提斯洋在全球范围内可能尚未完全关闭。从晚三叠世开始,新特提斯洋北侧一些原先从冈瓦纳大陆北缘裂离出来的微陆块开始与欧亚大陆南缘发生碰撞拼合,随后新特提斯洋开始向北俯冲并伴随着冈瓦纳大陆的进一步裂解,最终在新生代,裂解出来的板块(如非洲-阿拉伯板块、印度板块)与欧亚大陆碰撞,新特提斯洋最终闭合,形成全球瞩目的阿尔卑斯-扎格罗斯-喜马拉雅造山带 (朱日祥等, 2022)。位于秦 (岭)-祁 (连)-昆 (-仑) 中央造山带之内的东昆仑祁漫塔格地区被确认为地质历史上原特提斯洋和古特提斯洋闭合消减的产物 (Yu et al., 2021; 李文渊, 2024),这为研究原特提斯洋和古特提斯洋构造演化提供了天然实验室。

2 东昆仑原、古特提斯岩浆作用和斑岩成矿

2.1 东昆仑祁漫塔格成矿带构造演化

祁漫塔格成矿带东西长约 550 km,位于东昆仑造山带的西段,东起乌图美仁乡一带,西至阿尔金断裂,北与柴达木盆地相邻,西南与库木库里盆地相接 (钟世华, 2018)(图 2)。作为特提斯成矿域的一部分,东昆仑祁漫塔格地区(主要位于东昆北地体东段)在早古生代—中生代经历了复杂的构造演化历史,记录了原特提斯洋和古特提斯洋从裂解、扩张、俯冲到闭合的过程 (钟世华, 2018; Zhong et al., 2021b; Hu et al., 2023; Dong et al., 2024)。前人研究表明,祁漫塔格地区所在的东昆北地体在古生代早期可能属于原特提斯洋(在该地区又称为祁漫塔格洋)中的一个增生楔,随后大约在 520 Ma,原特提斯洋开始向南俯冲 (Li et al., 2018b; Song et al., 2018),并在 435.7 Ma 最终闭合进入同碰撞阶段 (陆济璞等, 2005),东昆北地体最终拼贴到东昆中地体,而后者此时为冈瓦纳大陆北缘的组成部分。黑山蛇绿岩(陈隽璐等, 2004)和十字沟蛇绿岩(宋泰忠等, 2010)是该地区原特提斯洋存在的直接证据。从同碰撞转入后碰撞的时限目前仍不清楚,但大量研究表明,原特提斯洋闭合后产生的后碰撞构造作用一直持续到约 370 Ma (寇贵存等, 2017; 张耀玲等, 2018; Duan et al., 2019; 张春宇等, 2019)。古特提斯洋在该地区的出现可能发生在晚泥盆世,而鸭子泉蛇绿岩(杨金中等, 1999)被认为是古特提斯洋的残片。此外,东昆南缝合带代表的勉略洋和阿尼玛卿缝合带记录的阿尼玛卿洋也是古特提斯洋的一部分 (Jia et al., 2018; Li et al., 2018b)。在 306 Ma 左右,古特提斯洋开始向北俯冲 (陆济璞等, 2005),在大约 245 Ma,古特提斯洋最终发生闭合 (Liu et al., 2005; Xiong et al., 2012; Xia et al., 2015),东昆中、东昆北地体最终与柴达木地体拼贴到一起。古特提斯洋闭合后的碰撞过程何时结束还存在不同认识,但现有研究表明,后碰撞岩浆作用

至少持续到 196 Ma(李洪普等, 2011)。

无论是原特提斯洋还是古特提斯洋, 在祁漫塔格地区俯冲阶段均很少发育弧岩浆作用, 出露的岩浆岩(特别是花岗岩类)年龄主要集中在 435~370 Ma 和 245~196 Ma(Zhong et al., 2021b)(图 3), 与 2 个古大洋闭合后的碰撞阶段对应。事实上, 在世界上许多碰撞造山带均发现了这种现象。例如, 在西阿尔卑斯造山带, Piemonte-Liguria 和 Valais 洋盆经历了长达 80 Ma 的俯冲消减, 然而在此过程中几乎没有弧岩浆作用发生 (Van Staal et al., 2015)。许多机制因此被提出, 用来解释这一现象, 如平板俯冲 (Bergomi et al., 2015)、缓慢的斜俯冲 (Van Staal et al., 2015)、大洋岩石层拖曳窄条陆壳俯冲等 (McCarthy et al., 2018)。对于祁漫塔格地区, 平板俯冲模型被更多学者接受 (Dong et al., 2018; Yu et al., 2020)。俯冲过程中, 大洋板片不断发生脱水, 释放的流体亏损 Nb、Ta, 富集高场强元素、大离子亲石元素和金属元素(如铜、铁)。这些富含金属的流体不断交代大陆岩石圈地幔和下地壳底部, 实现金属预富集, 为碰撞阶段斑岩-矽卡岩矿床形成提供了有利的源区条件 (Zhong et al., 2021b)。另外, 板片俯冲过程中, 上覆的沉积物可能随之发生俯冲, 这些沉积物通常具有典型的陆壳成分特征 (Bonin, 2004), 表现为富水、高氧逸度, 因此从这些沉积物中释放的流体会对碰撞阶段岩浆的同位素、氧逸度和水含量产生显著影响 (Gerrits et al., 2019)。不过, 根据祁漫塔格地区碰撞花岗岩类低氧逸度和低含水量的特征(见下文讨论), 笔者认为 2 个古大洋在俯冲消减过程中, 上覆的沉积物滞留在俯冲带增生楔位置, 没有跟随板片进入到深部地幔。年代学结果显示, 在 2 个古大洋闭合之前, 弧岩浆作用似乎有所增强, 这可能是俯冲板片后撤导致的 (Spakman and Hall, 2010)。

与俯冲阶段不同, 2 个古大洋闭合后, 碰撞岩浆作用均大规模爆发。这种现象通常是由软流圈物质上涌导致的, 而俯冲板片断离和后撤 (Atherton and Ghani, 2002; Zhang et al., 2014)、下地壳加厚 (He et al., 2011) 和拆沉 (Zhang et al., 2017b) 均可以触发软流圈物质上涌。另外, 地幔中残留俯冲洋壳的部分熔融也可以触发大规模的碰撞岩浆作用。对于到底哪一种机制造成祁漫塔格地区大规模碰撞岩浆作用的发生还存在争议, 但结合碰撞花岗岩类特征, 笔者认为板片断离模型似乎更加可信 (Zhong et al., 2021b)。板片断离造成软流圈物质上涌, 导致受俯冲流体交代的下地壳部分熔融并析出熔体, 熔体运移过程中经历了充分的 AFC 过程(即同化混染-结晶分异过程), 最终在祁漫塔格地区形成大量碰撞花岗岩类岩体。

根据以上特征, 祁漫塔格地区的原、古特提斯洋

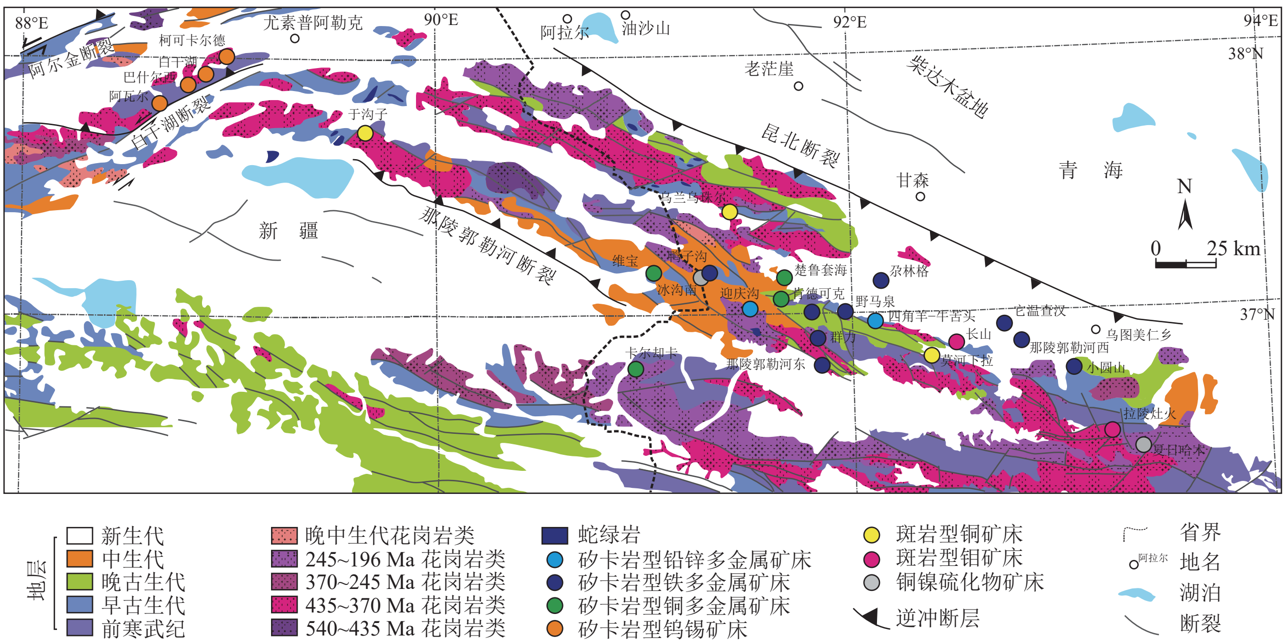

图 2　东昆仑祁漫塔格成矿带地质图 (据 Zhong et al., 2021b 修改)

Fig. 2　Geological map of the Qimantagh metallogenic belt

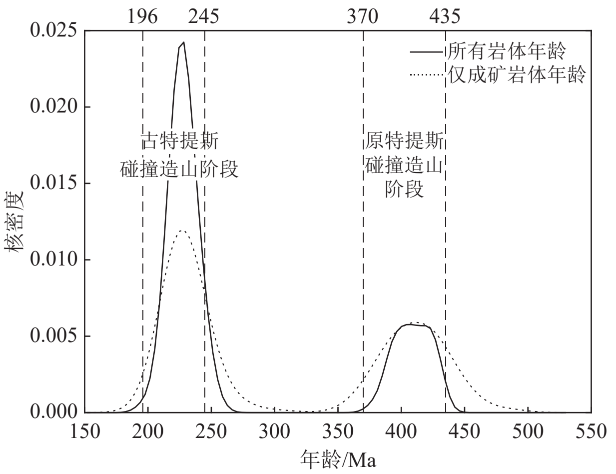

图 3 东昆仑祁漫塔格地区出露岩浆岩和成矿花岗岩年龄核密度图解(成矿岩体数据来源见表 1)

Fig. 3 Kernal density diagram for exposed magmatic rocks and ore-forming granitoids from the Qimantagh area

构造演化模型可以概括为以平板俯冲为主的大洋俯冲过程和以板片断离为特征的碰撞过程(图 4)。在俯冲阶段,平板俯冲抑制了弧岩浆作用的产生,导致原、古特提斯弧岩浆岩在祁漫塔格地区均相对匮乏。不同于俯冲阶段,碰撞开始后,板片断离诱发软流圈地幔物质上涌,导致大规模碰撞岩浆作用发生,因此原、古特提斯洋闭合后形成的碰撞花岗岩类在祁漫塔格地区十分发育。

2.2 斑岩-矽卡岩矿床特征

祁漫塔格地区迄今已经发现超过 30 个斑岩-矽卡岩矿床(点),以中小型为主,均形成于 2 个古大洋闭合后的碰撞阶段(表 1)。除个别矿床外(如乌兰乌珠尔矿床围岩为似斑状花岗闪长岩),大部分矿床的矿体出现在花岗岩类与碳酸盐岩类地层的交界处,含矿地层包括古—中元古界金水口群白沙河组、中元古界蓟县系狼牙山组、奥陶系—志留系滩间山群及石炭系缔敖苏组、大干沟组(丰成友等, 2010)。矽卡岩矿床主要包括 4 种类型:矽卡岩铜铅锌矿床(如维宝、虎头崖)、矽卡岩铁矿床(如尕林格)、矽卡岩铅锌矿床(如景忍-迎庆沟)和矽卡岩钨锡矿床(如白干湖)。其中,矽卡岩钨锡矿床主要出现在白干湖断裂和阿尔金断裂之间,形成了著名的白干湖钨锡矿田(李洪茂等, 2006; 王增振等, 2014; Deng et al., 2018),其矿床成因和构造演化过程可能与祁漫塔格地区主体部分不同,因此本文除非特别说明,所提及的斑岩-矽卡岩矿床不包括矽卡岩钨锡矿床。其他 3 种矽卡岩矿床类型之间没有明确的界线。越来越多的地质调查资料表明,祁漫塔格地区的矽卡岩矿

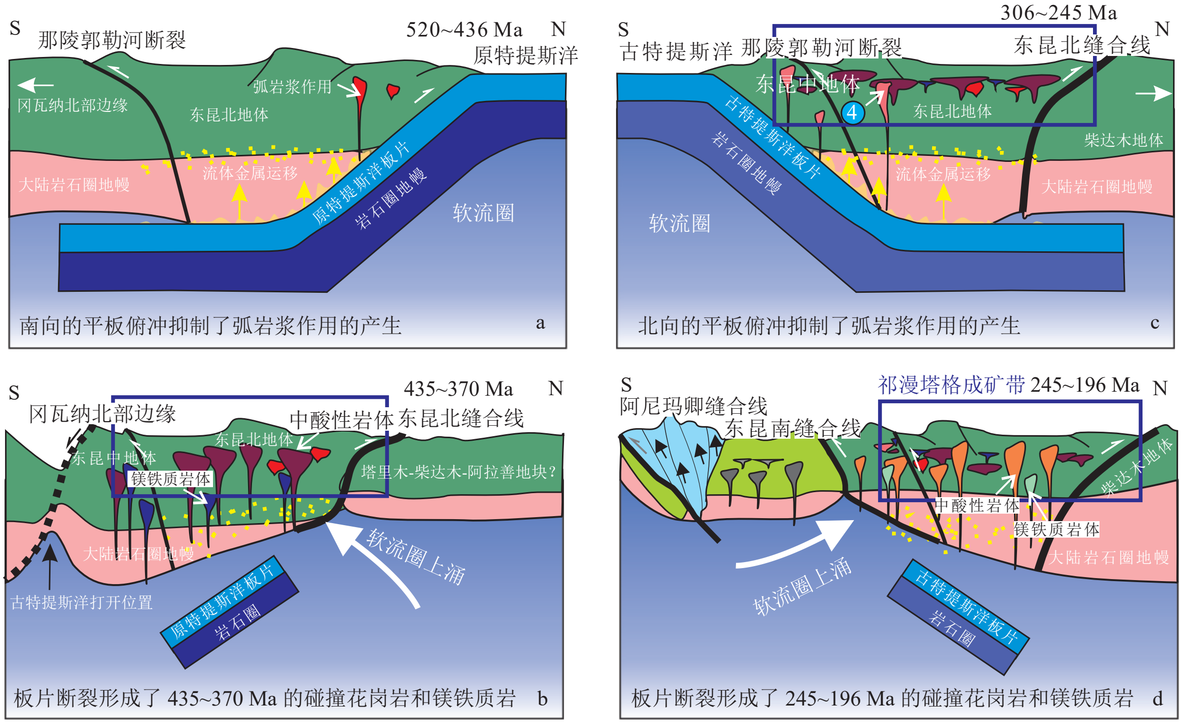

图 4 东昆仑祁漫塔格成矿带构造演化模式图 (据 Zhong et al., 2021b 修改)

Fig. 4 Chematic cartoon showing tetonic evolutionary histroy of the Qimantagh area

表 1　东昆仑祁漫塔格地区主要斑岩-矽卡岩矿床成岩成矿年龄

Table 1　Intrusive and mineralization ages for major porphyry-skarn deposits from the Qimantagh area, East Kunlun Mountains

矿床或矿点	矿床类型	采样位置	矿带	样品描述	定年矿物	定年方法	年龄/Ma	参考文献
柯可卡尔德	矽卡岩钨锡矿床	37°57'36.0"N; 88°56'21.9"E		二长花岗岩	锆石	LA−ICP−MS	429.5±3.2	高永宝, 2013
		37°57'30"N; 88°56'23"E		正长花岗岩	白云母	Ar−Ar	411.7±2.6	Zhou et al., 2016
		37°57'36"N; 88°56'24"E		黑钨矿-白云母-石英脉	白云母	Ar−Ar	412.8±2.4	
		37°57'28"N; 88°56'26"E		黑钨矿-白云母-石英脉	白云母	Ar−Ar	413.8±2.6	
		37°57'31.7"N; 88°56'26.7"E		锡石-石英脉	锡石	LA−MC−ICP−MS	426±13	Deng et al., 2018
		37°57'31.7"N; 88°56'26.7"E		锡石-石英脉	锡石	ID−TIMS	416±1	
				矿石	锡石	LA−MC−ICP−MS	427±13	高永宝, 2013
白干湖	矽卡岩钨锡矿床			二长花岗岩	锆石	LA−ICP−MS	431.3 ± 4.0	Zheng et al., 2018
		37°56'18"N; 88°54'21"E		二长花岗岩	锆石	LA−ICP−MS	428.2±4.2	王冠等, 2014
		37°55'24"N; 88°52'44"E		正长花岗岩	锆石	LA−ICP−MS	422.5±2.3	
		37°56'13"N; 88°54'44"E		正长花岗岩	锆石	LA−MC−ICP−MS	413.6±2.4	Zhou et al., 2016
巴什尔西	矽卡岩钨锡矿床			二长花岗岩	锆石	LA−ICP−MS	433.2 ± 3.4	Zheng et al., 2018
		ZK1202		黑钨矿-锡石-白云母脉	白云母	Ar−Ar	422.7±4.5	郑震等, 2016
				黑钨矿-锡石-白云母脉	白云母	Ar−Ar	421.8±2.7	
夏勒赛	矽卡岩钨锡矿床	37°47'51.3"N; 88°42'25.4"E		更长花岗岩	锆石	LA−ICP−MS	429.5±3.3	高永宝等, 2012
野马泉	矽卡岩铁矿	36°59'27.9"N; 91°56'51.6"E	M3	二长闪长岩	锆石	LA−ICP−MS	226.5±3.6	刘建楠, 2018
		ZK6461	M13	二长花岗岩	锆石	LA−ICP−MS	400.5±1.4	Chen et al., 2018
			M1	闪长岩	锆石	LA−ICP−MS	228±3	Yin et al., 2017
			M1	斑状花岗闪长岩	锆石	LA−ICP−MS	225±2	
			M1	斑状花岗闪长岩	锆石	LA−ICP−MS	221±2	
			M1	矿石	金云母	Ar−Ar	225±1.5	
		ZK11304	M3	二长岩	锆石	LA−ICP−MS	223.5±1.7	Yao , 2015
		36°58'37"N; 91°58'06"E	M1	二长花岗岩	锆石	LA−MC−ICP−MS	223.3±0.5	Zhang et al., 2017a
		37°00'09"N; 91°59'13"E	M5	石英二长闪长岩	锆石	LA−MC−ICP−MS	220.11±0.49	
		ZK10029, 602m	M13	花岗闪长岩	锆石	LA−ICP−MS	402.4±1.3	
		36°58'29.5"N; 91°58'19.6"E	M1	斑状二长花岗岩	锆石	LA−ICP−MS	229.5±2.2	刘建楠, 2018
		36°58'28.2"N; 92°01'33.8"E	M13	花岗闪长岩	锆石	LA−ICP−MS	402.8±5.4	
		X: 16413522; *Y*: 4095325	M13	花岗闪长岩	锆石	LA−ICP−MS	392.4±2.2	Song et al., 2014
		ZK507	M5	矿石	金云母	Ar−Ar	222.0±1.3	刘建楠, 2018
		ZK6801	M13	二长花岗岩	锆石	LA−ICP−MS	393±2	高永宝等, 2014
		ZK6057	M13	花岗闪长岩	锆石	LA−ICP−MS	386±1	
		36°59'20"N; 91°58'09"E	M1	斑状石英二长花岗岩	锆石	LA−ICP−MS	219±1	
		36°58'30"N; 91°58'20"E	M1	正长花岗岩	锆石	LA−ICP−MS	213±1	
			M13	花岗闪长岩	锆石	LA−ICP−MS	400.8±1.4	乔保星等, 2016
			M13	花岗闪长岩	锆石	LA−ICP−MS	220.53±0.69	
		ZK50101	M1	二长花岗岩	锆石	LA−ICP−MS	226.0 ± 1.9	Zhong et al., 2021a
		ZK50101	M1	二长花岗岩	锆石	LA−ICP−MS	226.2 ± 2.6	
		36°58'29.04"N; 91°58'20.33"E	M1	正长花岗岩	锆石	LA−ICP−MS	231.5 ± 1.6	
		ZK4863	M13	花岗闪长岩	锆石	LA−ICP−MS	405.0 ± 3.4	
		ZK6453	M13	花岗闪长岩	锆石	LA−ICP−MS	397.5 ± 3.1	
		ZK6805	M13	花岗闪长岩	锆石	LA−ICP−MS	390.5 ± 2.8	
		ZK6449	M13	二长花岗岩	锆石	LA−ICP−MS	406.3 ± 3.4	
		ZK9605	M13	二长花岗岩	锆石	LA−ICP−MS	396.2 ± 3.1	
		ZK6061	M13	花岗闪长岩	锆石	LA−ICP−MS	397.4 ± 3.4	

续表 1-1

矿床或矿点	矿床类型	采样位置	矿带	样品描述	定年矿物	定年方法	年龄/Ma	参考文献
它温查汗	矽卡岩铁矿			花岗闪长斑岩	锆石	LA-ICP-MS	233.5±0.9	Yao et al., 2017
		36°57'09.81"N; 92°44'58.66"E		花岗闪长斑岩	锆石	LA-MC-ICP-MS	236.0±2.3	杨涛等, 2017
		36°57'09.81"N; 92°44'58.66"E		二长花岗斑岩	锆石	LA-MC-ICP-MS	229.9±2.0	
		ZK25401		矿石	白云母	Ar-Ar	230.7±2.0	田承盛等, 2013
				花岗岩	锆石	LA-ICP-MS	227.7±0.6	丰成友等, 2012
于沟子	矽卡岩铁矿	37°43'6.1"N; 89°40'57.1"E		矿石	辉钼矿	Re-Os	210.1± 4.8	丰成友等, 2010
		37°43'06.21" N; 89°41'00.91" E		正长花岗岩	锆石	LA-ICP-MS	210.0±0.6	高永宝, 2013
小圆山	矽卡岩铁矿	ZK6703		英云闪长岩	锆石	LA-MC-ICP-MS	217.7±1.1	孔会磊等, 2016
				斜长花岗斑岩	锆石	LA-MC-ICP-MS	216.9±1.9	孔会磊等, 2015
那陵郭勒河西	矽卡岩铁矿	36°52'50.7"N; 92°49'54.48"E		闪长岩	锆石	LA-MC-ICP-MS	240.5±1.7	张雷, 2013
		36°50'50.4"N; 92°50'43.68"E		花岗斑岩	锆石	LA-MC-ICP-MS	227±1	
		36°50'50.4"N; 92°50'43.68"E		花岗斑岩	锆石	LA-MC-ICP-MS	229.51±0.87	
那陵郭勒河东	矽卡岩铁矿			正长花岗岩	锆石	LA-ICP-MS	225.2±1.2	薛宁等, 2009
		36°48.309'N; 92°51.585'E		闪长二长花岗岩岩	锆石	LA-ICP-MS	420.6±2.6	郝娜娜, 2014
尕林格	矽卡岩铁矿	37°07'34"N; 92°09'35"E	Ⅰ	石英二长闪长岩	锆石	LA-ICP-MS	228.3±0.5	高永宝等, 2012
		37°06'31"N; 92°11'04"E	Ⅲ	石英二长岩	锆石	LA-ICP-MS	234.4±0.6	
		ZK0307	Ⅱ	矿石	金云母	Ar-Ar	235.8±1.7	于淼等, 2015
		ZK0404	Ⅱ	辉石闪长岩	锆石	LA-ICP-MS	228.2±2	白宜娜等, 2016
			Ⅱ	闪长岩	锆石	LA-ICP-MS	223.4±2.7	于淼, 2017
			Ⅱ	闪长岩	锆石	LA-ICP-MS	219.56±0.89	
			Ⅳ	闪长岩	锆石	LA-ICP-MS	218.2±1.1	
			Ⅰ	花岗闪长岩	锆石	LA-ICP-MS	229.51±0.56	
			Ⅱ	花岗闪长岩	锆石	LA-ICP-MS	229.38±0.79	
			Ⅳ	花岗闪长岩	锆石	LA-ICP-MS	226.2±1.5	
			Ⅳ	闪长玢岩	锆石	LA-ICP-MS	217.6±1.0	
			Ⅴ	闪长玢岩	锆石	LA-ICP-MS	226.4±3.7	
肯德可克	矽卡岩铁钴矿			矿石	石榴子石	LA-ICP-MS	234 ± 4	Su et al., 2024
				矿石	榍石	LA-ICP-MS	231.8 ± 7.5	
				矿石	金云母	Ar-Ar	214	Wu et al., 2011
				二长花岗岩	锆石	LA-MC-ICP-MS	229.5±0.5	肖晔等, 2013
		37°00'45.7"N; 91°49'24.9"E		二长花岗岩	锆石	LA-ICP-MS	230.5±4.2	奚仁刚等, 2010
				辉长岩	斜长石	Ar-Ar	207.8±1.9	赵财胜等, 2006
		36°55.33'N; 91°40.17'E		二长花岗岩	锆石	LA-MC-ICP-MS	218±2	吴祥珂等, 2011
群力	矽卡岩铁矿			透辉石矽卡岩	白云母	Ar-Ar	407±2.8	何书跃等, 2018
牛苦头	矽卡岩铅锌矿	ZK1609		黑云母花岗闪长岩	锆石	LA-ICP-MS	393.7±4.9	李加多等, 2019
				花岗闪长岩	锆石	LA-ICP-MS	394.0±1.3	姚磊等, 2016
			M1	花岗闪长岩	锆石	LA-ICP-MS	362.2±2.7[a]	王新雨等, 2023
			M1	二长花岗岩	锆石	LA-ICP-MS	361.8±3.4[a]	
			M1	矿石	黄铁矿	Re-Os	359.2±6.3[a]	
			M1	斑状花岗岩	锆石	LA-ICP-MS	222.7±2.2	王新雨等, 2024
			M1	矿石	石榴子石	LA-ICP-MS	219±12	
四角羊				黑云母二长花岗岩	锆石	K-Ar	196	李洪普等, 2011

续表 1-2

矿床或矿点	矿床类型	采样位置	矿带	样品描述	定年矿物	定年方法	年龄/Ma	参考文献
景忍-迎庆沟	矽卡岩铅锌矿			正长花岗岩	锆石	SHRIMP	204.1±2.6	刘云华等, 2006
		37°1'36.36"N; 91°31'25.26"E		正长花岗斑岩	锆石	LA–MC–ICP–MS	221.1±1.3	张爱奎, 2013
		37°4'21.12"N; 91°45'1.68"E		花岗岩	锆石	LA–MC–ICP–MS	232.74±0.92	
		37°4'21.12"N; 91°45'1.68"E		花岗岩	锆石	LA–MC–ICP–MS	232.9±1.5	
		37°37'08"N; 91°30'49"E		二长花岗斑岩	锆石	LA–ICP–MS	211.6±1.4	韩海臣等, 2018
虎头崖	矽卡岩铜铅锌矿			矿石	磷灰石	LA–ICP–MS	443.0±5.9	张斌武, 2022
				二长花岗岩	磷灰石	LA–ICP–MS	228.1±1.5	
				钾长花岗岩	磷灰石	LA–ICP–MS	228.9±2.8	
				矿石	磷灰石	LA–ICP–MS	228.7±2.8	
		37°03'50.5"N; 91°40'37.5"E	Ⅵ	斑状二长花岗岩	锆石	LA–ICP–MS	232.3±1.4	Zhong et al., 2021b
		37°04'10.5"N; 91°39'37.6"E	Ⅲ	斑状二长花岗岩	锆石	LA–ICP–MS	230.3±1.5	
		37°04'01.9"N; 91°37'12.5"E	Ⅱ	二长花岗岩	锆石	LA–ICP–MS	221.6±0.7	
		X: 16383205; Y: 415100	Ⅵ	二长花岗岩	锆石	LA–MC–ICP–MS	217.5±1.1	张爱奎等, 2013
		37°03'44"N; 91°39'51"E	Ⅰ & Ⅲ	花岗闪长岩	锆石	SHRIMP	235.4±1.8	丰成友等, 2011
		37°04'09"N; 91°37'23"E	Ⅱ	二长花岗岩	锆石	LA–ICP–MS	219.2±1.4	
		37°05'20"N; 91°36'05"E	Ⅴ	矿石	辉钼矿	Re–Os	225.0±4.0	
		37°03'19"N; 91°38'01"E	Ⅶ	矿石	辉钼矿	Re–Os	230.1±4.7	
			Ⅲ	二长花岗岩	锆石	LA–MC–ICP–MS	230.3±3.7	瞿泓滢等, 2015
		37°05'16"N; 91°36'00"E	Ⅴ	花岗闪长岩	锆石	LA–MC–ICP–MS	224.3±0.6	李侃等, 2015
		ZK1501	Ⅷ	正长花岗岩	锆石	LA–MC–ICP–MS	239.7±0.8	姚磊, 2015
		ZK1901	Ⅵ	花岗岩	锆石	LA–MC–ICP–MS	233.6±1.8	
		ZK001	Ⅵ	花岗斑岩	锆石	LA–ICP–MS	232.7±1.8	张晓飞等, 2016
		37°4'21.3"N; 91°41'28.7"E	Ⅵ	斑状黑云母二长花岗岩	锆石	LA–ICP–MS	234.2±1.5	时超等, 2017
			?	二长花岗岩	锆石	LA–MC–ICP–MS	221.0±3.4	汪洋, 2017
			Ⅰ	二长花岗岩	锆石	LA–ICP–MS	235.0±1.5	姚磊, 2015
			Ⅱ	花岗岩	锆石	LA–ICP–MS	231.7±2.7	
			Ⅵ	二长花岗斑岩	锆石	LA–ICP–MS	222.8±2.6	
楚鲁套海	矽卡岩铜铅锌矿			花岗闪长岩	锆石	SIMS	226.4±1. 7	丰成友等, 2012
维宝	矽卡岩铜铅锌矿			矿石	白云母	Ar–Ar	226.61±2.34	Fang et al., 2018
		37°09.984'N; 91°04.462'E		石英闪长岩	锆石	LA–ICP–MS	223.3±1.5	钟世华, 2018
		37°06.114'N; 91°11.254'E		辉石闪长岩	锆石	SIMS	224.6±2.9	
卡而却卡	矽卡岩铜铅锌矿		?	花岗闪长岩	锆石	SHRIMP	237±2	王松等, 2009
		X:16323846; Y:4071935	B	斑状黑云母二长花岗岩	锆石	LA–ICP–MS	410.1±2.6	陈博等, 2012
			B	矿石	辉钼矿	Re–Os	238.8±1.3	丰成友等, 2009
		36°48'06.6"N; 90°58'33.3"E	C	花岗闪长岩	锆石	LA–ICP–MS	234.4±0.6	高永宝, 2013
		36°46'34"N; 90°04'54"E	B	花岗闪长岩	锆石	LA–ICP–MS	244.0±1.4	姚磊, 2015
		36°48'59.4"N; 90°58'35.3"E	B	斑状二长花岗岩	锆石	LA–ICP–MS	242.1±1.2	Zhong et al., 2021b
		ZK, M1-11 28.5m	?	花岗闪长岩	锆石	LA–ICP–MS	211.8±1.1	
		36°45'39"N; 91°01'51"E	B	斑状黑云母二长花岗岩	锆石	LA–ICP–MS	406.4±4.2	姚磊等, 2016
		36°45'39.6"N; 91°01'54.1"E	B	矿石	辉钼矿	Re–Os	245.5±1.6	高永宝等, 2018
		36°45'42.1"N; 91°01'44.1"E	B	矿石	金云母	Ar–Ar	233.9±1.4	
			C	花岗闪长岩	锆石	LA–ICP–MS	245.1±1.5	Yao et al., 2017
	斑岩铜矿	91°01'06"N; 36°45'48"E	A	斑状黑云母二长花岗岩	锆石	SHRIMP	227.3±1.8	丰成友, 2012
			A	斑状二长花岗岩	锆石	LA–ICP–MS	220.42±0.79	李积清等, 2016
		36°48'41"N; 90°58'26"E	A	斑状二长花岗岩	锆石	LA–ICP–MS	226.5±0.5	张勇等, 2017

续表 1-3

矿床或矿点	矿床类型	采样位置	矿带	样品描述	定年矿物	定年方法	年龄/Ma	参考文献
骆驼峰	斑岩铜矿			正长花岗岩	锆石	LA-ICP-MS	218±2	顾焱等, 2019
				花岗闪长岩	锆石	LA-ICP-MS	233±2	
鸭子沟	斑岩铜矿			花岗斑岩	锆石	SHRIMP	224.0±1.6	李世金等, 2008
				矿石	辉钼矿	Re-Os	224.7±3.4	丰成友等, 2009
莫河下拉	斑岩铜矿	11MZK08		花岗斑岩	锆石	LA-ICP-MS	222±1	许庆林, 2014
乌兰乌珠尔	斑岩铜矿	37°23'41"N; 91°25'53"E		斑状钾长花岗岩	锆石	LA-MC-ICP-MS	388.9±3.7	郭通珍等, 2011
		ZK701		花岗斑岩	锆石	SHRIMP	215.1±4.5	佘宏全等, 2007
				二长花岗岩	锆石	LA-ICP-MS	413±5	谈生祥等, 2011
长山	斑岩钼矿	ZK3101		正长花岗岩	锆石	SHRIMP	219.9±1.3	丰成友等, 2012
拉陵灶火中游	斑岩钼矿	36°31.715′N; 93°14.957′E		斑状钾长花岗岩	锆石	LA-ICP-MS	216.1±3.0	吴宗昌, 2017
		36°31.715′N; 93°14.957′E		斑状花岗岩	锆石	LA-ICP-MS	216.1±2.4	
		36°30'59"N; 93°17'35"E		矿石	辉钼矿	Re-Os	214.5±4.9	王富春等, 2013
		36°30'51"N; 93°17'35"E		矿石	辉钼矿	Re-Os	240.8±4.0	
				花岗岩	锆石	LA-MC-ICP-MS	228.49±0.84	严玉峰, 2012
		36°31'09"N; 93°18'15"E		花岗闪长岩	锆石	LA-ICP-MS	242.6±3.4	Chen et al., 2015
小灶火	斑岩钼矿			正长花岗岩	锆石	LA-ICP-MS	226±1	陈静等, 2018
拉陵沟脑	斑岩钼矿	36°24'12"N; 93°18'05"E		花岗闪长岩	锆石	LA-ICP-MS	238.6±2.9	Chen et al., 2015

注: 上标a代表报道的年龄可能存在问题, 见3.2节讨论

床大都为铁铜铅锌多金属矿床。例如, 牛苦头矿床曾被作为该地区铅锌矿床的典型代表, 而随着矿山揭露程度的提高, 新发现了大量的铁铜矿化 (赵子烨, 2019), 并且深部铁铜找矿前景巨大。除矽卡岩矿床外, 前人也在该地区报道了一些斑岩铜矿(如卡而却卡 A 区、乌兰乌珠尔、鸭子沟)和斑岩钼矿(如长山、拉陵灶火中游)(佘宏全等, 2007; 何书跃等, 2009; 赵淑芳等, 2014; 吴宗昌, 2017; 高永宝等, 2018)。然而, 这些斑岩型矿床大都规模很小, 缺少典型的面型矿化蚀变特征。另外, 对卡而却卡、乌兰乌珠尔的地质调查显示, 这些矿床不发育典型斑岩铜矿的“细脉浸染状”矿化类型, 石英网脉也相对不发育, 铜主要出现在构造破碎带中。显然, 对祁漫塔格地区的斑岩矿床还需要进一步深入研究。

祁漫塔格地区长期被作为三叠纪成矿大爆发的典型案例 (毛景文等, 2012)。近些年来的地质调查显示, 该地区的成矿历史可能更复杂。与许多典型斑岩成矿系统类似, 祁漫塔格地区的斑岩-矽卡岩矿床常见多期次、多类型花岗岩体在矿区范围内共存。例如, 根据钻孔揭露和年代学研究结果, 野马泉矽卡岩铁铜多金属矿床存在早—中泥盆世和晚三叠世 2 期后碰撞岩浆作用, 并且每一期岩浆活动根据年龄又可进一步细分 (Zhong et al., 2021a)。复杂的岩浆活动对矿床形成起到了促进作用, 但也增加了识别成矿岩体时的难度。例如在许多矿床中到底哪些岩体与成矿有关, 哪些是非成矿岩体, 还存在很大争议。特别是, 虽然在许多矿床均发育原特提斯和古特提斯碰撞花岗岩类岩体, 但是由于原特提斯地质记录被晚期古特提斯造山旋回不同程度叠加改造, 加之难以找到合适的定年对象, 导致理清 2 期碰撞岩浆岩类与成矿作用的关系尚存在一定难度。

近些年来, 随着地质调查与研究的深入, 一些矿床陆续报道了志留纪—泥盆纪的成矿年龄(表 1), 如何书跃等 (2018) 获得群力铁矿透辉石矽卡岩中云母 Ar−Ar 年龄为 407±2.8 Ma, 证明该地区存在与原特提斯碰撞造山有关的一期成矿事件。另外, 研究发现, 435~370 Ma 和 245~196 Ma 2 期碰撞花岗岩类成分相似, 具有一致的岩浆起源和演化路径(见后文介绍), 这也支持无论原特提斯造山作用, 还是古特提斯造山作用, 均可形成斑岩-矽卡岩矿床。

2.3 2 期碰撞花岗岩类特征

考虑到已发现的斑岩-矽卡岩矿床均与原特提斯和古特提斯 2 个古大洋闭合后的碰撞岩浆作用有关, 因此, 在此只讨论 435~370 Ma 和 245~196 Ma 2 期碰撞岩浆岩的特征和成因, 并分别将其命名为原特提斯碰撞花岗岩和古特提斯碰撞花岗岩。

岩相学上, 2 期碰撞花岗岩类十分类似, 岩石类型主要为花岗闪长岩、二长花岗岩和钾长花岗岩, 以斑状和似斑状结构为主, 其次为中细粒结构。不过, 相比于原特提斯碰撞花岗岩, 古特提斯碰撞花岗岩中常见暗色微粒包体 (Yao et al., 2020)。化学成分上, 2 期碰撞花岗岩类也十分类似, 在 SiO_2−K_2O 图解(图 5−a, b)上, 样品点主要落入高钾钙碱性系列范围, 其次为钾玄岩系列, 并且大多数样品的 A/CNK 值小于 1.1, 属于偏铝质—弱过铝质岩石(图 5−c, d)。在稀土元素球粒陨石标准化配分曲线上, 2 期碰撞花岗岩均表现出右倾型特点, 轻稀土元素富集, 重稀土元素相对亏损, 并且具有不同程度的负 Eu 异常(图 6−a, b)。古特提斯碰撞花岗岩的 Eu 异常程度高于原特提斯碰撞花岗岩, 可能暗示前者经历了更明显的斜长石分异结晶。另外, 2 期碰撞花岗岩表现出 Nb、Ta、Ti 亏损特征(图 6−c, d), 与弧花岗岩类似, 指示源区受到了弧岩浆的混染。

原特提斯碰撞花岗岩的 ε_{Nd} 值为−2.1~−0.1(均值为−0.9), 初始$^{87}Sr/^{86}Sr$ 值为 0.7030~0.7074(均值为 0.7050), 锆石 ε_{Hf} 值变化范围为−2.4±2.0~+3.8±1.2(1σ), 对应的二阶段 Nd 模式年龄为 1155~1858 Ma, 二阶段 Hf 模式年龄为 944~1733 Ma(Zhong et al., 2021b)。古特提斯碰撞花岗岩的 ε_{Nd} 值为−7.4~+0.1(均值为−4.5), 初始$^{87}Sr/^{86}Sr$ 值为 0.7086~0.7167, 锆石 ε_{Hf} 值为−4.7±1.6(1σ)~+2.5±1.1(1σ), 对应的二阶段 Nd 模式年龄为 1165~1614 Ma, 二阶段 Hf 模式年龄为 1001~1670 Ma(Zhong et al., 2021b)。可以看出, 2 期碰撞花岗岩类的 Sr−Nd−Hf 同位素特征十分类似, 指示它们具有类似的源区。另外, 在图 7 上, 2 期碰撞花岗岩类均落入由金沙江大洋中脊玄武岩(代表亏损软流圈地幔)和金水口群花岗岩(代表中元古代变硬砂岩)作为地幔和陆壳源区端元组成的混合曲线上。略微不同的是, 原特提斯碰撞花岗岩的源区组成中, 亏损地幔端元所占的比重更

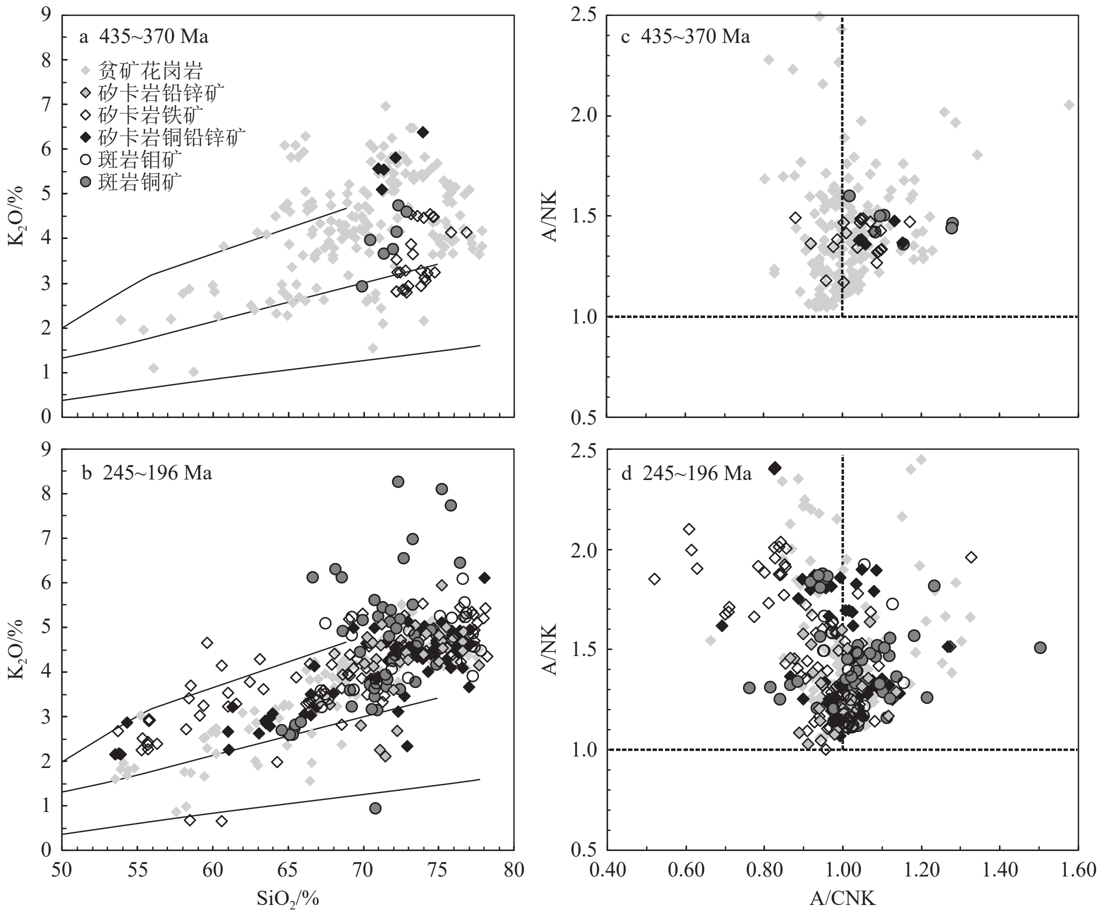

图 5　东昆仑祁漫塔格地区 2 期碰撞花岗岩类全岩 SiO_2−K_2O(a,c) 和 A/CNK−A/NK(b,d) 图解

Fig. 5　Whole-rock SiO_2−K_2O(a,c) and A/CNK−A/NK(b,d) diagrams for two suites of collisional granitoids from the Qimantagh area, East Kunlun Mountains

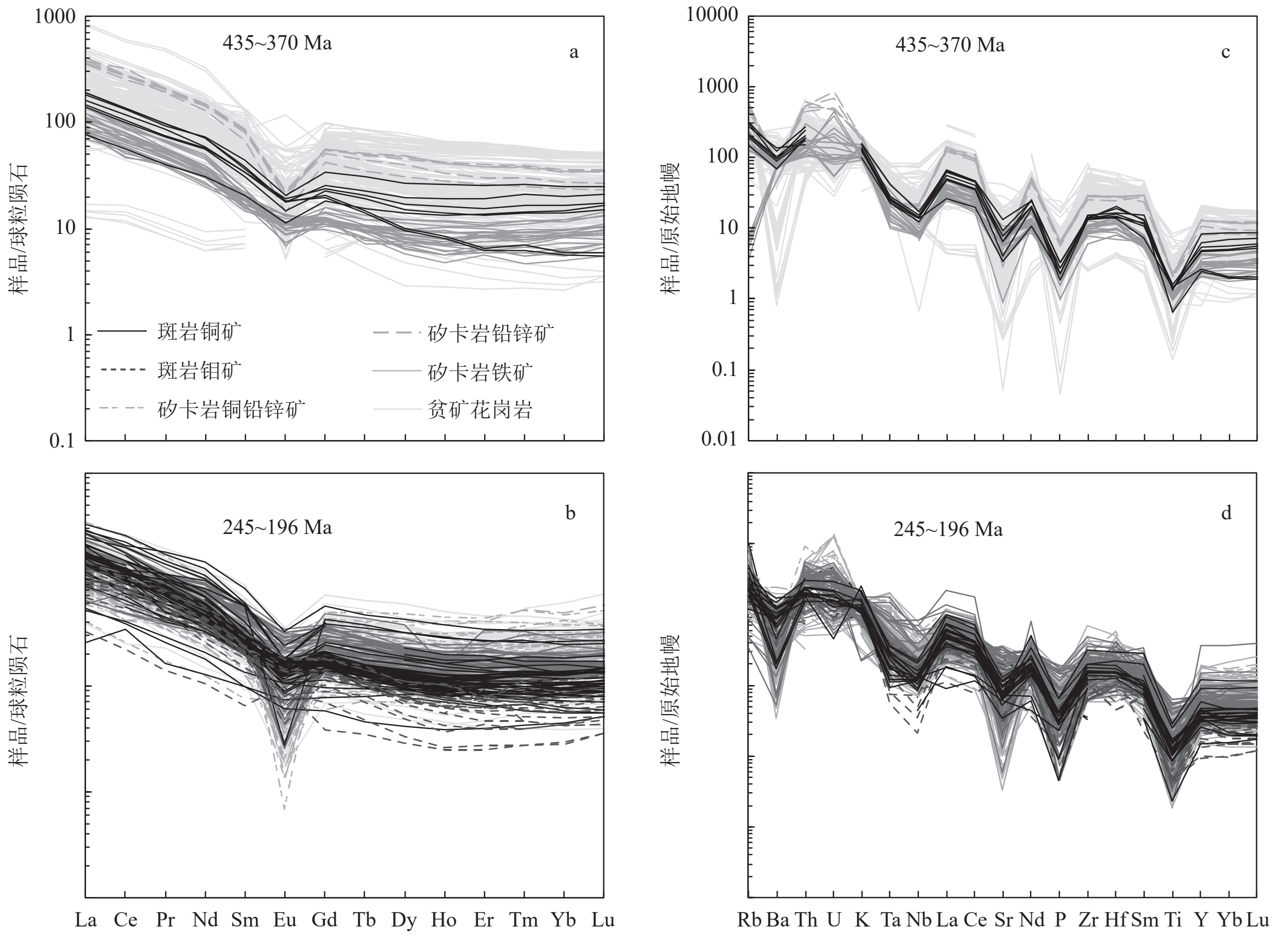

图 6 东昆仑祁漫塔格地区 2 期碰撞花岗岩类全岩微量元素图解

Fig. 6 Whole-rock trace element diagrams for two suites of collisional granitoids from the Qimantagh area, East Kunlun Mountains

大，为 70%~90%，而亏损地幔端元对古特提斯碰撞花岗岩的贡献为 60%~85%。

无论全岩主量和微量元素，还是稳定同位素，2 期碰撞花岗岩类中成矿岩体和非成矿岩体均未表现出明显的差异（图 5—图 7），这与前人的研究结果一致，表明全岩成分不能很好地区分成矿岩体和非成矿岩体 (Ballard et al., 2002; Shu et al., 2019)。这是由于全岩成分极易受到后期热液活动的扰动 (Zhong et al., 2018)。此外，前已述及，祁漫塔格矿区内岩浆活动十分频繁，加之研究程度不高，一些成矿岩体可能被误当作非成矿岩体，反过来亦然，这可能也在一定程度上掩盖了地球化学图解上成矿岩体和非成矿岩体之间的差异。

3 区域找矿方向

3.1 2 期碰撞岩浆斑岩铜矿成矿潜力

长期以来，东昆仑祁漫塔格地区被认为是斑岩铜矿的潜在找矿靶区 (袁万明等, 2017)，并投入了大量的调查与勘查工作。2 期碰撞花岗岩类也的确表现出一些斑岩铜矿成矿岩体的岩石学和地球化学特征。例如，2 期碰撞花岗岩类大部分属于分异的钙碱性系列闪长岩-花岗闪长岩，并且具有右倾型稀土元素配分模式，岩浆形成过程中经历了壳幔相互作用 (侯增谦等, 2007; Richards et al., 2012)。此外，2 期碰撞花岗岩类在主量元素上与来自冈底斯斑岩铜矿带的成矿岩体也十分类似 (Wang et al., 2018)。然而，在过去长达 20 多年的地质调查中，在该地区仅发现了乌兰乌珠尔、鸭子沟等几个小型的斑岩铜矿床（点），并且这些矿床缺乏典型斑岩铜矿的蚀变矿化特征。

为了进一步理清东昆仑祁漫塔格地区 2 期碰撞花岗岩类是否具有形成斑岩铜矿的潜力，图 8 对比了该地区斑岩-矽卡岩矿床成矿岩体与冈底斯斑岩铜矿带后碰撞斑岩铜矿成矿岩体的锆石成分。冈底斯

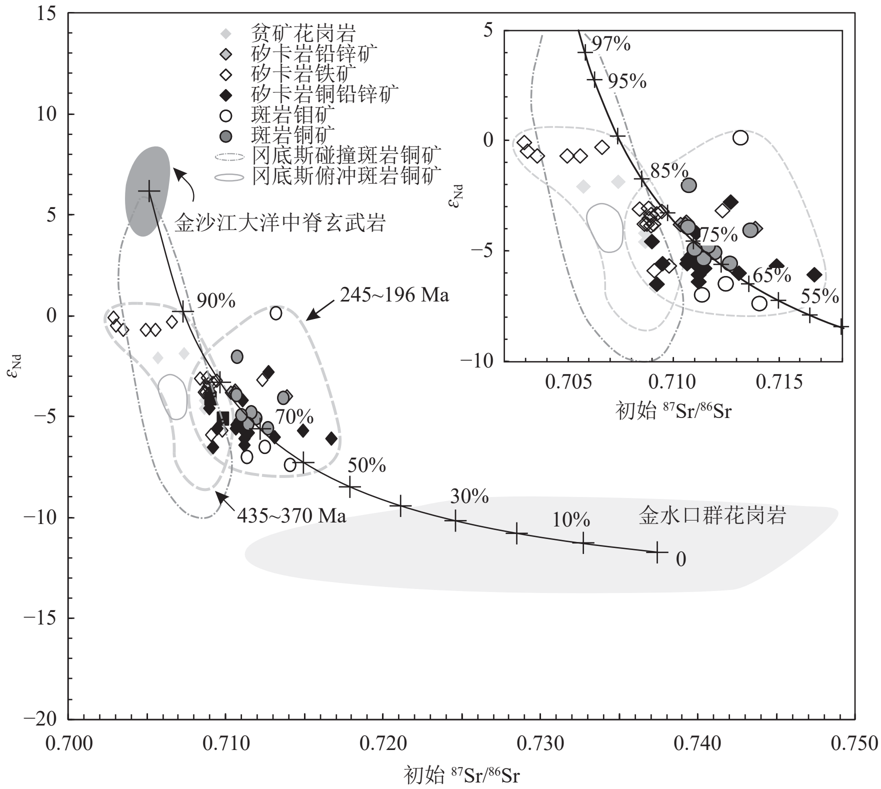

图 7　东昆仑祁漫塔格地区 2 期碰撞花岗岩类全岩 Sr−Nd 同位素图解(据 Zhong et al., 2021b 修改)

Fig. 7　Whole−rock Sr−Nd isotopic diagrams for two suites of collisional granitoids from the Qimantagh area, East Kunlun Mountains

斑岩铜矿带发育驱龙、甲玛等大型—超大型斑岩铜矿，主要形成于新特提斯洋闭合后的碰撞阶段，因此与之对比可以更好地阐明祁漫塔格地区碰撞环境斑岩铜矿成矿潜力，揭示原特提斯和古特提斯造山作用与新特提斯造山作用的异同，指导特提斯成矿域斑岩铜矿找矿勘查。本次选取锆石作为对比工具，是由于锆石成分稳定、不易受到后期热液活动扰动，且锆石成分被证实能够很好地指示岩浆氧逸度和含水量 (Zhong et al., 2019; 杜立华等, 2024; 黄宇等, 2025)，而大量的研究表明，氧化还原条件和含水量是识别岩体成矿能力的重要指标，斑岩铜矿床通常是由氧化(ΔFMQ +1~+2)、富水的岩浆形成的 (Shen et al., 2015; Li et al., 2019; Meng et al., 2021; Zhu et al., 2022)。可以看出，2 期碰撞花岗岩类与冈底斯斑岩铜矿带成矿岩体特征显著不同。特别是，祁漫塔格地区成矿岩体锆石 Eu/Eu*值明显低于冈底斯成矿岩体(图 8−a, b)。2 个成矿带的锆石 Ce/Ce*值虽然较接近，但冈底斯成矿岩体总体上仍呈现出更高的比值。锆石 Ce/Ce*值与岩浆氧逸度成正比，而 Eu/Eu*值受岩浆氧逸度和含水量共同控制，高氧逸度和高含水量均可以降低锆石的负异常程度。此外，根据 Loucks et al.(2020) 的方法，本文进一步限定了冈底斯斑岩铜矿带和祁漫塔格地区成矿岩体的氧逸度。可以看出，冈底斯碰撞斑岩铜矿成矿岩体的氧逸度大都位于 FMQ+1~FMQ+2 范围内，而祁漫塔格地区 2 期碰撞花岗岩类氧逸度大都位于 FMQ 曲线以下。综上所述，锆石特征指示，祁漫塔格地区斑岩-矽卡岩矿床成矿岩体相对还原，氧逸度低于冈底斯斑岩铜矿带成矿岩体，而二者的含水量差异更大，祁漫塔格斑岩-矽卡岩矿床成矿岩浆明显相对贫水。综合当前祁漫塔格地区的找矿实践，以上特征可能指示该地区发育大型—超大型斑岩铜矿的先天条件不足。

需要指出的是，虽然祁漫塔格地区可能不具有形成大型—超大型斑岩铜矿的潜力，但是大型—超大型矽卡岩铁铜铅锌多金属矿床找矿潜力仍旧巨大，小型斑岩铜矿也可能被陆续发现。这是由于相对于大型—超大型斑岩铜矿，矽卡岩矿床和小型斑岩铜矿形成过程中，金属运移和富集对岩浆氧逸度

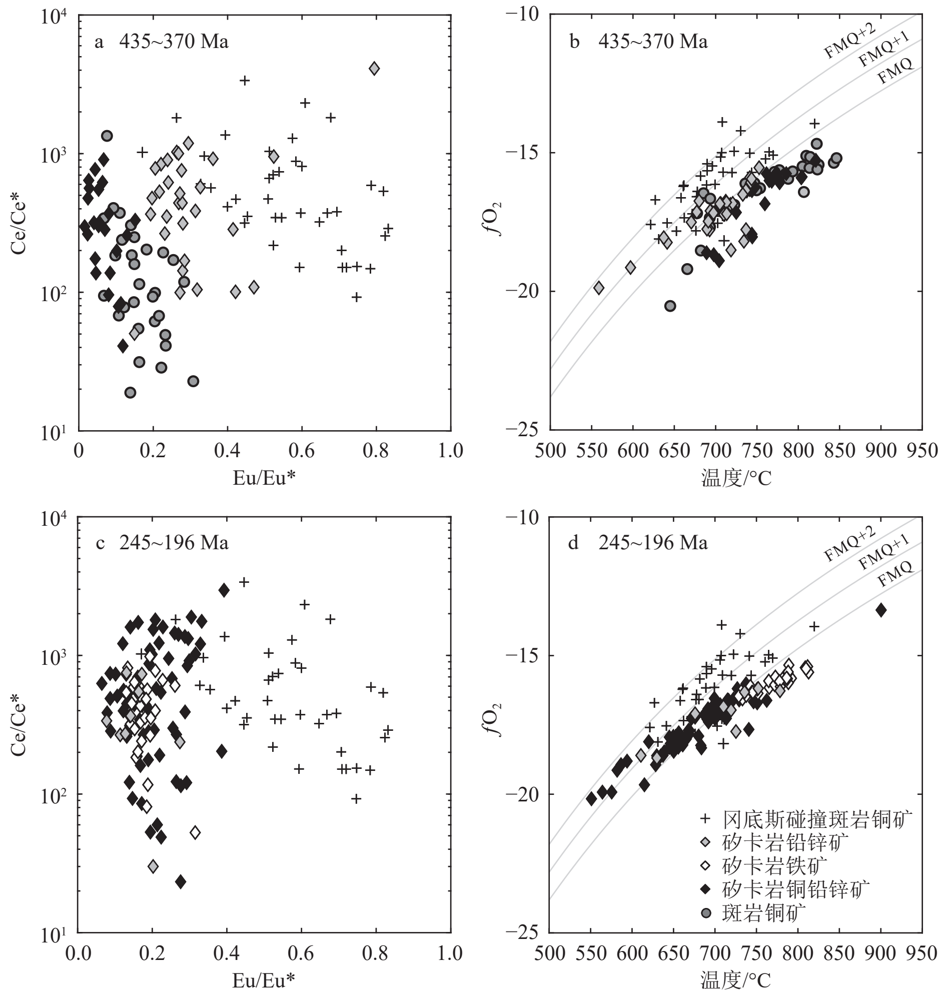

图 8 祁漫塔格地区斑岩-矽卡岩矿床成矿岩体与冈底斯斑岩铜矿带碰撞斑岩铜矿成矿岩体锆石成分对比
（冈底斯锆石数据据 Wang et al., 2018; 祁漫塔格锆石数据据 Zhong et al., 2021; Eu/Eu*和 Ce/Ce*计算据 Zhong et al., 2019; f_{O_2} 计算据 Loucks et al., 2020; FMQ 曲线据 O'Neill, 1987）

Fig. 8 Zircon composition comparisons for fertile rocks from the porphyry-skarn deposits in the Qimantagh area and the porphyry Cu deposits from the Gangdese Cu belt

和水含量的要求可能要低一些 (Zhong et al., 2018, 2021b)。最近,尕林格、牛苦头等矽卡岩矿床的外围和深部找矿取得新突破,矿床规模进一步扩大,也证明该地区矽卡岩矿床找矿前景巨大。

3.2 志留纪—泥盆纪斑岩-矽卡岩矿床找矿前景

前已述及,以往认为祁漫塔格地区发育的斑岩-矽卡岩铁铜铅锌矿床(不包括白干湖等钨锡矿床)形成于三叠纪,即由古特提斯造山作用形成,因此长期以来工业界和学术界均重点关注三叠纪花岗岩,而对原特提斯造山过程中斑岩-矽卡岩成矿潜力研究很少。目前,越来越多的研究指出,在原特提斯洋闭合后的碰撞阶段,即志留纪—泥盆纪,也可以形成斑岩-矽卡岩矿床 (高永宝等, 2014; 宋忠宝等, 2014; 姚磊等, 2016),但是这一观点远未形成共识。主要原因是前人把在斑岩-矽卡岩矿床中发现志留纪—泥盆纪岩体,并在这些岩体中发现铜铁铅锌多金属矿化作为本地区存在另一期成矿事件的最重要证据,但事实上这些矿化极有可能是由晚期(中—晚三叠世)成矿叠加造成的。这是由于几乎在所有报道存在志留纪—泥盆纪斑岩-矽卡岩矿化的矿床(如野马泉),大都同时存在强烈的三叠纪岩浆-成矿作用 (Zhong et al., 2021a)。其次,作为确定成矿时代的最直接证据,来自斑岩-矽卡岩矿石的辉钼矿 Re-Os 年龄和热液矿物(如云母)Ar-Ar 年龄大都为三叠纪,只有何书跃等 (2018) 报道群力铁矿床矽卡岩中热液白云母年龄为 407.0±2.8 Ma,张斌武 (2022) 报道虎头崖矿床铜

铅锌矿石中热液磷灰石年龄为 433.0±5.9 Ma。尽管如此,通过系统对比 435~370 Ma 和 245~196 Ma 两期碰撞花岗岩类,表明它们在岩相学和地球化学成分上非常相似(图 5—图 8)。这一证据支持了祁漫塔格地区志留纪—泥盆纪也具有发育斑岩-矽卡岩矿床潜力的观点。

笔者认为,祁漫塔格地区许多斑岩-矽卡岩矿床可能均由 2 期碰撞岩浆共同形成。之所以目前报道的成矿年龄集中在三叠纪,是由于三叠纪岩浆-热液活动更强烈,其结果是一方面破坏了早期地质体,另一方面是破坏了早期热液矿物的封闭同位素体系,从而难以准确记录志留纪—泥盆纪成矿事件。例如,王新雨等 (2023) 最近报道了牛苦头矿床 M1 矿段花岗闪长岩和二长花岗岩锆石 U−Pb 年龄分别为 362.2±2.7 Ma(MSWD=2.2)和 361.8±3.4 Ma (MSWD=2.5),并获得与主成矿阶段闪锌矿共生的黄铁矿 Re−Os 年龄为 359.2±6.3 Ma(MSWD=45),并将获得的锆石 U−Pb 年龄作为成矿岩体就位年龄,将黄铁矿年龄作为矿化年龄。然而,王新雨等 (2023) 报道的成矿岩体年龄明显比前人报道的牛苦头对应期次的花岗岩年龄(393.7~400.7 Ma)(姚磊等, 2016;李加多等, 2019;耿健, 2023) 年轻。进一步研究发现,王新雨等 (2023) 报道的 2 个锆石 U−Pb 年龄加权平均值的 MSWD 均远大于 1,指示该年龄为混合年龄,并非真实年龄 (Siégel et al., 2018)。造成这一问题的一个可能原因是,在计算年龄加权平均值时未将发生铅丢失的锆石颗粒去除 (Lee et al., 2017)。黄铁矿年龄也存在同样问题,MSWD 高达 45,指示年龄不可靠,可能为混合成因。尽管如此,相对年轻的黄铁矿等时线年龄可以很好地被“早期热液矿物同位素体系被晚期热液活动扰动”解释,从而间接证明牛苦头矿床存在早泥盆世成矿事件,与前人报道的原特提斯碰撞花岗岩类时代一致。

综上,祁漫塔格地区志留纪—泥盆纪斑岩-矽卡岩矿床找矿潜力巨大,是实现西北地区铜铁多金属资源增储上产的重要突破口。未来找矿勘查和研究中,应着重调查志留纪—泥盆纪花岗岩类周边的蚀变-矿化情况,在选择定年矿物、解释成矿年龄时,要注意排除三叠纪岩浆-热液活动对早期成矿事件的干扰。另外,相比于祁漫塔格地区南部,以往对该地区北部的研究较少(于淼等, 2017),因此,在未来的研究中,应特别关注祁漫塔格地区北部志留纪—泥盆纪花岗岩类的分布及矿化情况。

4　结　论

(1)东昆仑祁漫塔格地区不但广泛出露早古生代—中生代不同时期的花岗岩类,同时发育许多斑岩-矽卡岩矿床,记录了原、古特提斯洋从俯冲到闭合阶段的构造演化过程和成矿历史,是研究原特提斯和古特提斯斑岩成矿作用的天然实验室和绝佳场所。

(2)原、古特提斯洋经历了类似的构造演化过程,俯冲阶段洋壳表现为平板俯冲,抑制了弧岩浆作用,碰撞阶段俯冲板片裂离导致软流圈地幔上涌,形成了丰富的碰撞花岗岩类,分别集中于 435~370 Ma 和 245~196 Ma 两个时期,它们具有类似的岩相学和化学成分特征,并且相对还原、贫水,可能不利于大型—超大型斑岩铜矿的形成。

(3)祁漫塔格地区存在 2 期斑岩-矽卡岩铁铜铅锌成矿事件,分别与 2 期碰撞花岗岩类的就位有关。未来该地区应以矽卡岩铜多金属矿床作为主攻找矿方向,并且加强对志留纪—泥盆纪花岗岩类成矿潜力的研究。

References

Atherton M P, Ghani A A. 2002. Slab breakoff: A model for Caledonian, Late Granite syn−collisional magmatism in the orthotectonic (metamorphic) zone of Scotland and Donegal, Ireland[J]. Lithos, 62(3/4): 65−85.

Bai Y N, Sun F Y, Qian Y, et al. 2016. Zircon U−Pb geochronology and geochemistry of pyroxene diorite in the Galinge iron−polymetallic deposit, East Kunlun[J]. Global Geology, (1): 17−27 (in Chinese with English abstract).

Ballard J R, Palin J M, Campbell I H. 2002. Relative oxidation states of magmas inferred from Ce (IV)/Ce (III) in zircon: Application to porphyry copper deposits of northern Chile[J]. Contributions to Mineralogy and Petrology, 144(3): 347−364.

Bergomi M A, Zanchetta S, Tunesi A. 2015. The Tertiary dike magmatism in the Southern Alps: Geochronological data and geodynamic significance[J]. International Journal of Earth Sciences, 104: 449−473.

Bonin B. 2004. Do coeval mafic and felsic magmas in post−collisional to within−plate regimes necessarily imply two contrasting, mantle and crustal, sources? A review[J]. Lithos, 78(1/2): 1−24.

Chen J, Wang B Z, Li B, et al. 2015. Zircon U–Pb ages, geochemistry, and Sr–Nd–Pb isotopic compositions of Middle Triassic granodiorites from the Kaimuqi area, East Kunlun, Northwest China: Implications for slab breakoff[J]. International Geology Review, 57(2): 257−270.

Chen J, Wang B Z, Lu H F, et al. 2018. Geochronology and geochemistry of Early Devonian intrusions in the Qimantagh area, Northwest China: Evidence for post-collisional slab break-off[J]. International Geology Review, 60(4): 479-95.

Chen B, Zhang Z Y, Geng J Z, et al. 2012. Zircon LA-ICP-MS U-Pb age of monzogranites in the Kaerqueka copper-polymetallic deposit of Qimantag, Western Qinghai Province[J]. Geological Bulletin of China, (2/3): 463-468 (in Chinese with English abstract).

Chen J, Hu J C, Lu Y Z, et al. 2018a. Geochronology, geochemical characteristics of molybdenum ore-bearing syenogranite from Xiaozhaohuo area in East Kunlun and its geological significance[J]. Gold Science and Technology, 26(4): 465-472 (in Chinese with English abstract).

Deng J, Wang Q, Li G, et al. 2014. Tethys tectonic evolution and its bearing on the distribution of important mineral deposits in the Sanjiang region, SW China[J]. Gondwana Research, 26(2): 419-437.

Deng X H, Chen Y J, Bagas L, et al. 2018. Cassiterite U-Pb geochronology of the Kekekaerde W-Sn deposit in the Baiganhu ore field, East Kunlun Orogen, NW China: Timing and tectonic setting of mineralization[J]. Ore Geology Reviews, 100: 534-544.

Deng Z, Zhong S, Yan J, et al. 2024. Magma mixing formed mineralized Middle–Late Triassic granitoids in the Qimantagh Metallogenic Belt, NW China: A case study from the Hutouya skarn deposit[J]. Ore Geology Reviews, 106192.

Ding L. 2024. New Advances in the Study of Tethyan Geodynamic System[J]. Science China Earth Sciences, 54(3): 892-896 (in Chinese with English abstract).

Dong Y, He D, Sun S, et al. 2018. Subduction and accretionary tectonics of the East Kunlun orogen, western segment of the Central China Orogenic System[J]. Earth-Science Reviews, 186: 231-261.

Dong Y, Sun S, He D, et al. 2024. Early Paleozoic back-arc basin in the East Kunlun Orogen, northern Tibetan Plateau: Insight from the Wutumeiren ophiolitic mélange[J]. Lithos, 464/465: 107460.

Du L H, Huang Y, Gao X, et al. 2025. Characteristics of strong reducing metallogenic porphyry and its constraints on the genesis of the rare metal-tin-polymetallic deposit in Weilasituo, Inner Mongolia [J]. Geological Bulletin of China, 44(4):633-648 (in Chinese with English abstract).

Duan X P, Meng F C, Jia L H. 2019. Early Paleozoic mantle evolution of East Kunlun Orogenic Belt in Qinghai, NW China: evidence from the geochemistry and geochronology of the Late Ordovician to Late Silurian mafic-ultramafic rocks in the Qimantag region[J]. International Geology Review, 62(15): 1883-1903.

Fang J, Zhang L, Chen H, et al. 2018. Genesis of the Weibao banded skarn Pb-Zn deposit, Qimantagh, Xinjiang: Insights from skarn mineralogy and muscovite $^{40}Ar-^{39}Ar$ dating[J]. Ore Geology Reviews, 100: 483-503.

Feng C Y, Wang S, Li G C, et al. 2012. Middle to Late Triassic granitoids in the Qimantage area, Qinghai Province, China: Chronology, geochemistry and metallogenic significances[J]. Acta Petrologica Sinica, 28(2): 665-678 (in Chinese with English abstract).

Feng C Y, Li D S, Qu W J, et al. 2009. Re-Os Isotopic dating of molybdenite from the Suolajier skarn-type copper-molybdenum deposit of Qimantage Mountain in Qinghai Province and its geological significance[J]. Rock and Mineral Analysis, 28(3): 223-227 (in Chinese with English abstract).

Feng C Y, Li D S, Wu Z S, et al. 2010. Major types, time-space distribution and metallogenesis of polymetallic deposits in the Qimantagh metallogenic belt, Eastern Kunlun Area[J]. Northwestern Geology, 43(4): 10-17 (in Chinese with English abstract).

Feng C Y, Wang X P, Shu X F. et al. 2011. Isotopic chronology of the Hutouya skarn lead-zinc polymetallic ore district in the Qimantage area of Qinghai Province and its geological significance[J]. Journal of Jilin University (Earth Science Edition), 41(6): 1806-1817 (in Chinese with English abstract).

Fu H, Han J H, Sun Y X, et al. 2024. Tethys orogenic belt[J]. Sedimentary Geology and Tethyan Geology, 44(1): 100-133 (in Chinese with English abstract).

Gao Y B, Li K, Qian B, et al. 2018. The metallogenic chronology of Kaerqueka deposit in Eastern Kunlun: Evidences from molybdenite Re-Os and phlogopite Ar-Ar ages[J]. Geotectonica et Metallogenia, 42(1): 96-107 (in Chinese with English abstract).

Gao Y B, Li W Y, Ma X G, et al. 2012a. Genesis, geochronology and Hf isotopic compositions of the magmatic rocks in Galinge iron deposit, eastern Kunlun[J]. Journal of Lanzhou University (Natural Sciences), 48(2): 36-47 (in Chinese with English abstract).

Gao Y B, Li W Y, Li K, et al. 2012b. Genesis and chronology of the Baiganhu-Jialesai W-Sn mineralization belt, Qimantage, East Kunlun Mountain, NW China[J]. Northwestern Geology, 45(4): 229-241 (in Chinese with English abstract).

Gao Y B. 2013. The intermediate-acid intrusive magmatism and mineralization in Qimantag, East Kunlun Mountains[D]. Doctoral Thesis of Chang'an University (in Chinese with English abstract).

Gao Y B, Li W Y, Qian B, et al. 2014. Geochronology, geochemistry and Hf isotopic compositions of the granitic rocks related with iron mineralization in Yemaquan deposit, East Kunlun, NW China[J]. Acta Petrologica Sinica, 30(6): 1647-1665 (in Chinese with English abstract).

Geng J. 2023. Study on magmatic rocks and mineralization of two stage in Niukutou Mining area, Qinghai Province[D]. Master Thesis of China University of Geosciences (Beijing) (in Chinese with English abstract).

Gerrits A R, Inglis E C, Dragovic B, et al. 2019. Release of oxidizing fluids in subduction zones recorded by iron isotope zonation in garnet[J]. Nature Geoscience, 12: 1029-1033.

Gu Y, Qian Y, Li Y J, et al. 2019. Geochronology, geochemistry, and tectonic significance of Middle and Late Triassic granites in the Luotuofeng area, East Kunlun[J]. Mineral Exploration, 10(4): 724-736 (in Chinese with English abstract).

Guo G H, Zhong S H, Li S Z, et al. 2023. Constructing discrimination diagrams for granite mineralization potential by ssing machine learning and zircon trace elements: Example from the Qimantagh, East Kunlun[J]. Northwestern Geology, 56(6): 57-70 (in Chinese with English abstract).

Guo T, Liu R, Chen F, et al. 2011. LA−MC−ICP−MS zircon U−Pb dating of Wulanwuzhuer porphyritic syenite granite in the Qimantagh Mountain of Qinghai and its geological significance[J]. Geological Bulletin of China, (8): 1203−1211 (in Chinese with English abstract).

Han H C, Wang G L, Ding Y J, et al. 2018. LA−ICP−MS zircon U−Pb age of late Triassic intrusive rocks in Bayinhudousen area, East Kunlun and its tectonic significance[J]. Northwestern Geology, 51(1): 144−58 (in Chinese with English abstract).

Hao N N, Yuan W M, Zhang A K, et al. 2014b. Late Silurian to Early Devonian granitoids in the Qimantage Area, East Kunlun Mountains: LA−ICPMS zircon U–Pb ages, geochemical features and geological setting[J]. Geological Review, 60(1): 201−15 (in Chinese with English abstract).

He Y, Li S, Hoefs J, et al. 2011. Post−collisional granitoids from the Dabie orogen: new evidence for partial melting of a thickened continental crust[J]. Geochimica et Cosmochimica Acta, 75: 3815−3838.

He S Y, Bai G L, Liu Z G, et al. 2025. A preliminary discussion on the metallogenetic pattern of Qinghai Province[J/OL]. Geological Bulletin of China, 44(4): 649-678 (in Chinese with English abstract).

He S Y, Li D S, Bai G L, et al. 2018. The report on $^{40}Ar/^{39}Ar$ age of muscovite from the Qunli Fe−polymetallic deposit in the Qimantag area, Qinghai Province[J]. Geology in China, 45(1): 201−202 (in Chinese with English abstract).

He S Y, Li D S, Li L L, et al. 2009. Re−Os age of molybdenite from the Yazigou Copper (Molybdenum) mineralized area in Eastern Kunlun of Qinghai Province and its geological significance[J]. Geotectonica et Metallogenia, 33(2): 236−242 (in Chinese with English abstract).

He S Y, Lin G, Zhong S H, et al. 2023. Geological characteristics and related mineralization of"Qinghai Gold Belt" formed by orogeny[J]. Northwestern Geology, 56(6): 1−16 (in Chinese with English abstract).

Hou Z, Pan X, Yang Z, et al. 2007. Porphyry Cu–(Mo–Au) deposits not related to oceanic−slab subduction: examples from Chinese porphyry deposits in continental settings[J]. Geoscience, 21: 332−351 (in Chinese with English abstract).

Hou Z, Zheng Y, Yang Z, et al. 2012. Contribution of mantle components within juvenile lower−crust to collisional zone porphyry Cu systems in Tibet[J]. Mineralium Deposita, 48: 173−192.

Hou Z Q. 2010. Metallogensis of continental collision[J]. Acta Geologica Sinica, 84(1): 30−58 (in Chinese with English abstract).

Hou Z Q, Pan X F, Yang Z M, et al. 2007. Porphyry Cu−(Mo−Au) deposits no related to oceanic slab subduction: Examples from Chinese porphyry deposits in continental−settings[J]. Geoscience, (2): 332−351 (in Chinese with English abstract).

Hu C, Li M, Feng C, et al. 2023. Petrogenesis and metallogenic potential of the early Devonian Yugusayi mafic−ultramafic complex in Qimantagh, East Kunlun orogenic belt[J]. International Geology Review, 65: 1056−1076.

Jia L, Meng F, Feng H. 2018. The Wenquan ultramafic rocks in the Central East Kunlun Fault zone, Qinghai−Tibet Plateau—crustal relics of the Paleo−Tethys ocean[J]. Mineralogy and Petrology, 112: 317−339.

Kong H L, Li J C, Huang J, et al. 2015. Zircon U−Pb dating and geochemical characteristics of the plagiogranite porphyry from the Xiaoyuanshan iron−polymetallic ore district in East Kunlun Mountains[J]. Geology in China, 42(3): 521−533 (in Chinese with English abstract).

Kong H L, Li J C, Li Y Z, et al. 2016. LA−MC−ICP−MS zircon U−Pb dating and its geological implications of the tonalite from Xiaoyuanshan iron−polymetallic ore district in Qimantage Mountain, Qinghai Province[J]. Geologcal Science and Technology Information, 35(1): 8−16 (in Chinese with English abstract).

Kou G C, Feng J W, Luo B, et al. 2017. Zircon U−Pb dating and geochemistry of the volcanic rocks from Maoniushan Formation in Amunike area, Qinghai Province, and its geological implications[J]. Geological Bulletin of China, 36(2/3): 275−284 (in Chinese with English abstract).

Lee R G, Dilles J H, Tosdal R M, et al. 2017. Magmatic evolution of granodiorite intrusions at the El Salvador porphyry copper deposit, Chile, based on trace element composition and U/Pb age of zircons[J]. Economic Geology, 112: 245−273.

Li C S, Zhang Z W, Li W Y, et al. 2015a. Geochronology, petrology and Hf–S isotope geochemistry of the newly−discovered Xiarihamu magmatic Ni–Cu sulfide deposit in the Qinghai–Tibet plateau, western China. Lithos, 216/217: 224−240.

Li J Q, Chen J, Shi Q R, et al. 2016. The genesis of porphyritic monzogranite of the Kaerqueka deposit in the East Kunlun: Evidence from zircon U–Pb dating and Sr–Nd isotopic compositions[J]. Journal of Mineralogy and Petrology, 36(3): 87−95 (in Chinese with English abstract).

Li H M, Shi Y D, Liu Z G, et al. 2006. Geological features and origin of the Baigan Lake W−Sn deposit in the Ruoqiang area, East Kunlun Mountains, China[J]. Geological Bulletin of China, (2/3): 277−281 (in Chinese with English abstract).

Li H P, Liu J C, Zhang X Q, et al. 2011. Characteristics of magmatic rocks from the Sijiaoyang Fe−polymetallic ore district in the southern margin of Qaidam, Qinghai Province and their metallogenic significance[J]. Geology and Exploration, 47(6): 1009−1017 (in Chinese with English abstract).

Li J D, Wang X Y, Zhu X Y, et al. 2019. The preliminary discussion of the Hercynian metallogenic period in Qimantag area−with the example of Niukutou lead and zinc deposit[J]. Mineral Exploration, 10(8): 1775−1783 (in Chinese with English abstract).

Li K, Gao Y, Qian B, et al. 2015b. Geochronology, geochemical characteristics, and Hf isotopic compositions of granite in the Hutouya deposit, Qimantag, East Kunlun[J]. Geology in China, (3): 630−645 (in Chinese with English abstract).

Li S, Suo Y, Li X, et al. 2018. Microplate tectonics: new insights from micro−blocks in the global oceans, continental margins and deep mantle[J]. Earth−Science Reviews, 185: 1029−1064.

Li S, Zhao S, Liu X, et al. 2018. Closure of the Proto−Tethys Ocean and Early Paleozoic amalgamation of microcontinental blocks in East Asia[J]. Earth−Science Reviews, 186: 37−75.

Li S J, Sun F Y, Feng C Y, et al. 2008. Geochronological study on the

Yazigou polymetallic deposit in Eastern Kunlun, Qinghai Province[J]. Acta Geologica Sinica, 82(7): 949−955 (in Chinese with English abstract).
Li S Z, Zhao S J, Li X Y, et al. 2016. ProtoTehtys Ocean in East Asia (I): Northern and southern border faults and subduction polarity[J]. Acta Petrologica Sinica, 32(9): 2609−2627 (in Chinese with English abstract).
Li S Z, Zhao S J, Yu S, et al. 2016. Proto−Tehtys Ocean in East Asia (Ⅱ): Affinity and assmbly of Early Paleozoic micro−continental blocks[J]. Acta Petrologica Sinica, 32(9): 2628−2644 (in Chinese with English abstract).
Li W, Yang Z, Cao K, et al. 2019. Redox−controlled generation of the giant porphyry Cu–Au deposit at Pulang, southwest China[J]. Contributions to Mineralogy and Petrology, 174: 12.
Li W Y. The Paleo−Tethys tectonic evolution and Corresponding Metallogenesis[J/OL]. Acta Geologica Sinica, 1−19 (in Chinese with English abstract).
Li Z H, Cui F Y, Yang S T, et al. 2023. Key geodynamic processes and driving forces of Tethyan evolution[J]. Science China Earth Sciences, 53(12): 2701−2722 (in Chinese with English abstract).
Liu J N, Feng C Y, He S Y, et al. 2017. Zircon U−Pb and phlogopite Ar−Ar ages of the monzogranite from Yemaquan iron−zinc deposit in Qinghai Province[J]. Geotectonica et Metallogenia, 41(6): 1158−70 (in Chinese with English abstract).
Liu Y, Genser J, Neubauer F, et al. 2005. $^{40}Ar/^{39}Ar$ mineral ages from basement rocks in the Eastern Kunlun Mountains, NW China, and their tectonic implications[J]. Tectonophysics, 398: 199−224.
Liu J Q, Zhong S H, Li S Z, et al. 2023. Identification of mineralized and barren magmatic rocks for the pophryry−skarn deposits from the Qimantagh, East Kunlun: Based on machine learning and whole−Rock compositions[J]. Northwest Geology, 56(6): 41−56 (in Chinese with English abstract).
Loucks R R, Fiorentini M L, Henríquez G J, 2020. New magmatic oxybarometer using trace elements in zircon. Journal of Petrology 61, egaa034.
Lu J P, Li J, Qin X F, et al. 2005. The Yinieke'agan granite mass in Qimantag, eastern Kunlun and its tectonic significance[J]. Sedimentary and Tethyan Geology, (4): 46−54 (in Chinese with English abstract).
Lv P R, Yao W G, Zhang H S, et al. 2020. Petrogenesis, source, tectonic evolution and mineralization process of the Miocene porphyry Cu deposits in the Tethyan metallogenic domain[J]. Acta Geologica Sinica, 94(8): 2291−2310 (in Chinese with English abstract).
Mao J W, Zhou Z H, Feng C Y, et al. 2012. A preliminary study of the Triassic large−scale mineralization in China and its geodynamic setting[J]. Geology in China, 39(6): 1437−1471 (in Chinese with English abstract).
McCarthy A, Chelle−Michou C, Müntener O, et al. 2018. Subduction initiation without magmatism: The case of the missing Alpine magmatic arc[J]. Geology, 46: 1059−1062.
Meng X, Kleinsasser J M, Richards J P, et al. 2021. Oxidized sulfur−rich arc magmas formed porphyry Cu deposits by 1.88 Ga[J]. Nature Communications, 12(1): 2189.
Metcalfe I. 2013. Gondwana dispersion and Asian accretion: Tectonic and palaeogeographic evolution of eastern Tethys[J]. Journal of Asian Earth Sciences, 66: 1−33.
O'Neill H S C. 1987. Quartz−fayalite−iron and quartz−fayalite−magnetite equilibria and the free energy of formation of fayalite (Fe_2SiO_4) and magnetite (Fe_3O_4)[J]. American Mineralogist, 72(1/2): 67−75.
Peng B, Sun F Y, Li B L, et al. 2016. The geochemistry and geochronology of the Xiarihamu II mafic–ultramafic complex, Eastern Kunlun, Qinghai Province, China: Implications for the genesis of magmatic Ni–Cu sulfide deposits[J]. Ore Geology Reviews, 73: 13−28.
Qiao B, Pan T, Chen J. 2016. Geochronology, Geochemical characteristics, and geological significance of granodiorite in the Yemaquan iron polymetallic deposit of the East Kunlun, Qinghai Province[J]. Journal of Qinghai University (Natural Science Edition), (1): 63−73 (in Chinese with English abstract).
Qu H Y, Feng C Y, Pei R F, et al. 2015. Thermochronology of the Hutouya skarn−type copper−lead−zinc polymetallic ore district in the Qimantage Area, Qinghai Province[J]. Acta Geologica Sinica, (3): 498−509 (in Chinese with English abstract).
Qu H Y, Liu J N, Pei R F, et al. 2018. Thermochronology of the monzonitic granite related to the Hutouya Cu−Pb−Zn polymetallic deposit in Qiman Tage, Qinghai Province[J]. Geology in China, 45(3): 511−527 (in Chinese with English abstract).
Richards J P, Şengör A C. 2017. Did Paleo−Tethyan anoxia kill arc magma fertility for porphyry copper formation?[J]. Geology, 45: 591−594.
Richards J P, Spell T, Rameh E, et al. 2012. High Sr/Y magmas reflect arc maturity, high magmatic water content, and porphyry Cu±Mo±Au potential: examples from the Tethyan arcs of Central and Eastern Iran and Western Pakistan[J]. Economic Geology, 107: 295−332.
Şengör A C. 1979. Mid−Mesozoic closure of Permo–Triassic Tethys and its implications[J]. Nature, 279: 590−593.
She, H Q, Zhang D Q, Jing X Y, et al. 2007. Geological characteristics and genesis of the Ulan Uzhur porphyry copper deposit in Qinghai[J]. Geology in China, (2): 306−314 (in Chinese with English abstract).
Shen P, Hattori K, Pan H, et al. 2015. Oxidation Condition and Metal Fertility of Granitic Magmas: Zircon Trace−Element Data from Porphyry Cu Deposits in the Central Asian Orogenic Belt[J]. Economic Geology, 110: 1861−1878.
Shi C, Li R, He S, et al. 2017. A study of the ore−forming age of the Hutouya deposit and its geological significance: Geochemistry and U−Pb zircon ages of biotite monzonitic granite in Qimantag, East Kunlun Mountains[J]. Geological Bulletin of China, 36(6): 977−86 (in Chinese with English abstract).
Shu Q, Chang Z, Lai Y, et al. 2019. Zircon trace elements and magma fertility: insights from porphyry (−skarn) Mo deposits in NE China[J]. Mineralium Deposita, 54(5): 645−656.
Siégel C, Bryan S E, Allen C M, et al. 2018. Use and abuse of zircon−based thermometers: A critical review and a recommended approach to identify antecrystic zircons[J]. Earth−Science Reviews,

176: 87−116.

Song S, Bi H, Qi S, et al. 2018. HP–UHP Metamorphic belt in the East Kunlun Orogen: final closure of the Proto−Tethys ocean and formation of the Pan−North−China continent[J]. Journal of Petrology, 59: 2043−2060.

Song X Y, Yi J N, Chen L M, et al. 2016. The giant Xiarihamu Ni−Co sulfide deposit in the East Kunlun orogenic belt, Northern Tibet plateau, China[J]. Economic Geology, 111(1): 29−55.

Song Z B, Zhang Y L, Jia Q Z, et al. 2014. U−Pb age of Yemaquan deep variscan granodiorite in Qimantage area, Eastern Kunlun and its significance[J]. Geoscience, 28(6): 1161−1169 (in Chinese with English abstract).

Spakman W, Hall R. 2010. Surface deformation and slab–mantle interaction during Banda arc subduction rollback[J]. Nature Geoscience, 3: 562−566.

Su H M, Che Y Y, Liu T, et al. 2024. Multiple generations of garnet and their genetic significance in the Niukutou cobalt−rich Pb−Zn−(Fe) skarn deposit, East Kunlun orogenic belt, western China[J]. Ore Geology Reviews, 106308.

Tan S X, Guo T Z, Dong J S, et al. 2011. Geological characteristics and significance of the peraluminous granite in Late Silurian Epoch in Wulanwuzhuer region of Qinghai[J]. Journal of Qinghai University (Nature Science), 29(1): 36−43 (in Chinese with English abstract).

Tang J X. 2019. Mineral resources base investigation and research status of the Tibet Plateau and its adjacent majormetallogenic belts.[J]. Acta Petrologica Sinica, 35(3): 617−624 (in Chinese with English abstract).

Tang J X, Duoji, Liu H F, et al. 2012. Minerogenetic series of ore deposits in the east part of the Gangdise metallogenic Belt[J]. Acta Geoscientica Sinica, 33(4): 393−410.

Tian C S, Feng C Y, Li H J, et al. 2013. ^{40}Ar–^{39}Ar geochronology of Tawenchahan Fe−Polymetallic deposit in Qimantag mountain of Qinghai Province and its geological implications[J]. Mineral Deposits, (1): 169−176 (in Chinese with English abstract).

Van Staal C R, Wilson R A, McClelland W. 2015. Discussion: Taconian orogenesis, sedimentation and magmatism in the southern Quebec−northern Vermont Appalachians: Stratigraphic and detrital mineral record of Iapetan suturing[J]. American Journal of Science, 315: 486−500.

Wang R, Weinberg R F, Collins W J, et al. 2018. Origin of postcollisional magmas and formation of porphyry Cu deposits in southern Tibet[J]. Earth−Science Reviews, 181: 122−143.

Wang B Z, Pan T, Ren H D, et al. 2021. Cambrian Qimantagh island arc in the East Kunlun orogen: Evidences from zircon U−Pb ages, lithogeochemistry and Hf isotopes of high−Mg andesite/diorite from the Lalinggaolihe area[J]. Earth Science Frontiers, 28(1): 318−333 (in Chinese with English abstract).

Wang G, Sun F Y, Li B L, et al. 2014b. Petrography, zircon U−Pb geochronology, and geochemistry of the mafic−ultramafic intrusion in the Xiarihamu Cu−Ni deposit from East Kunlun, with implications for geodynamic setting[J]. Earth Science Frontiers, 21(6): 381−401 (in Chinese with English abstract).

Wang R, Zhu D C, Wang Q, et al. 2020. Porphyry mineralization in the Tethyan orogen[J]. Scientia Sinica (Terrae), 50(12): 1919−1946 (in Chinese with English abstract).

Wang S, Feng C Y, Li S J, et al. 2009. Zircon sHRIMP U−Pb dating of granodiorite in the Kaerqueka polymetallic ore deposit, Qimantage mountain, Qinghai Province, and its geological Implications[J]. Geology in China, 36(1): 74−84 (in Chinese with English abstract).

Wang X Y, Wang S, Liu M, et al. Study on the chronology and trace element characteristics of skarn mineral in the Niukutou Deposit, Qimantag region, Qinghai Province[J/OL]. Earth Science Frontiers: 1−27 (in Chinese with English abstract).

Wang Y. 2017. Study on the geological characteristics and enrichment regularities of mineralization of Hutouya copper−iron deposit, Qimantage, Qinghai Province[D]. Master Thesis of Jilin University: 1−58 (in Chinese with English abstract).

Wang Z Z, Han B F, Feng C Y, et al. 2014. Geochronology and geochemistry of granites in the Baiganhu Area, Xinjiang, and their tectonic implications[J]. Acta Petrologica et Mineralogica, 33(4): 597−616 (in Chinese with English abstract).

Wu F Y, Wan B, Zhao L, et al. 2020. Tethyan geodynamics[J]. Acta Petrologica Sinica, 36(6): 1627−1674 (in Chinese with English abstract).

Wu X K, Meng F C, Xu H, et al. 2011. Zircon U−Pb Dating, Geochemistry, and Nd−Hf Isotopic Compositions of the Maxingdaban Late Triassic Granitic Pluton from Qimantag in the Eastern Kunlun[J]. Acta Petrologica Sinica, 27(11): 3380−3394 (in Chinese with English abstract).

Wu Z C. 2017. Genesis and Exploration Prospect of the Bo Wu Porphyry Molybdenum Deposit in the East Kunlun Orogenic Belt[D]. Master Thesis of China University of Geosciences (Beijing) (in Chinese with English abstract).

Xi R G, Xiao P X, Wu Y Z, et al. 2010. The geological significances, composition, and age of the monzonitic granite in the Kendekeke iron mine[J]. Northwestern Geology, 43(4): 195−202 (in Chinese with English abstract).

Xia R, Wang C, Qing M, et al. 2015. Zircon U–Pb dating, geochemistry and Sr–Nd–Pb–Hf–O isotopes for the Nan'getan granodiorites and mafic microgranular enclaves in the East Kunlun Orogen: Record of closure of the Paleo−Tethys[J]. Lithos, 234/235: 47−60.

Xiao Y, Feng C Y, Liu J N, et al. 2013. M. LA−MC−ICP−MS zircon U−Pb dating and sulfur isotope characteristics of the Kendekeke Fe−polymetallic deposit, Qinghai Province[J]. Mineral Deposits, 32(1): 177−186 (in Chinese with English abstract).

Xin R C. 2024. Global Tethys tectonic domain and its spatiotemporal distribution[J/OL]. Sedimentary Geology and Tethyan Geology: 1−20 (in Chinese with English abstract).

Xiong F H, Ma C Q, Zhang J Y, et al. 2012. The origin of mafic microgranular enclaves and their host granodiorites from East Kunlun, Northern Qinghai−Tibet Plateau: implications for magma mixing during subduction of Paleo−Tethyan lithosphere[J]. Mineralogy and Petrology, 104: 211−224.

Xu B. 2019. Chronology, Geochemistry, and Tectonic Setting of Late Triassic Igneous Rocks in the Ageteng Area, Qimantage, Qinghai[D].

Master Thesis of Jilin University:1−48 (in Chinese with English abstract).

Xue N, An Y S, Li W F, et al. 2009. Characteristic and genesis of normal granite in the Yemaquan Area of Qinghai[J]. Journal of Qinghai University (Natural Science), 27(2): 18−22 (in Chinese with English abstract).

Yan Y F, Yang X S, Chen F B, et al. 2012. Molybdenum containing granites in Lalingzaohuo of the East Kunlun resources and environment[J]. Resources and Environment, 18(4): 37−39 (in Chinese with English abstract).

Yang T, Li Z M, Zhang L, et al. 2017. Geological and geochemical characteristics of the Tawenchahanxi granites in East Kunlun and its tectonic significance[J]. Geological Journal of China Universities, 23(3): 452−464 (in Chinese with English abstract).

Yao L, Dong S Y, Lü Z C, et al. 2020. Origin of the Late Permian gabbros and Middle Triassic granodiorites and their mafic microgranular enclaves from the Eastern Kunlun Orogen Belt: Implications for the subduction of the Palaeo−Tethys Ocean and continent–continent collision[J]. Geological Journal, 55: 147−172 (in Chinese with English abstract).

Yao L, Lü Z, Zhao C, et al. 2017. Zircon U–Pb geochronological, trace element, and Hf isotopic constraints on the genesis of the Fe and Cu skarn deposits in the Qiman Tagh area, Qinghai Province, Eastern Kunlun Orogen, China[J]. Ore Geology Reviews, 91: 387−403.

Yao L. 2015. Petrogenesis of the Triassic Granitoids and Skarn Mineralization in the Qimantag Area, Qinghai Province, and Their Geodynamic Setting[D]. Doctoral Thesis of China University of Geosciences (Beijing): 1−175(in Chinese with English abstract).

Yao L, Lv Z C, Zhao C S, et al. 2016a. Geochronological study of granitoids from the Niukutou and B section of the Kaerqueka deposits, Qimantag area, Qinghai Province: Implications for Devonian magmatism and mineralization[J]. Geological Bulletin, 35(7): 1158−1169 (in Chinese with English abstract).

Yao L, Lv Z C, Zhao C S, et al. 2016b. LA−ICP−MS zircon U−Pb dating of granitic rocks in the B zone of the Niukutou and Ka'erquka deposits, East Kunlun Qimantagh: implications for Devonian diagenesis and mineralization[J]. Geological Bulletin of China, 35(7): 1158−1169 (in Chinese with English abstract).

Yin S, Ma C, Xu J. 2017. Geochronology, geochemical and Sr–Nd–Hf–Pb isotopic compositions of the granitoids in the Yemaquan orefield, East Kunlun orogenic belt, northern Qinghai−Tibet Plateau: Implications for magmatic fractional crystallization and sub−solidus hydrothermal alteration[J]. Lithos, 294/295: 339−355.

Yu M, Dick J M, Feng C, et al. 2020. The tectonic evolution of the East Kunlun Orogen, northern Tibetan Plateau: A critical review with an integrated geodynamic model[J]. Journal of Asian Earth Sciences, 191: 104168.

Yu M, Feng C Y, He S Y, et al. 2017. The Qimantagh Orogen as a window to the crustal evolution of the northern Tibetan Plateau[J]. Acta Geologica Sinica, 91: 703−723 (in Chinese with English abstract).

Yu M. 2017. Geochemistry and zonation of the Galinge iron deposit, Qinghai Province[D]. Master Thesis of China University of Geosciences (Beijing): 106.

Yu M, Feng C, Liu H, et al. 2015. $^{40}Ar-^{39}Ar$ geochronology of the Galinge large skarn iron deposit in Qinghai Province and geological significance[J]. Acta Geologica Sinica, (3): 510−521 (in Chinese with English abstract).

Yu S, Peng Y, Zhang J, et al. 2021. Tectono−thermal evolution of the Qilian orogenic system: Tracing the subduction, accretion and closure of the Proto−Tethys Ocean[J]. Earth−Science Reviews, 215: 103547.

Yuan W M, Mo X X, Zhang A K, et al. 2017. Discovery of new porphyry belts in Eastern Kunlun Mountainsl Oinghai: Tibet Plateau[J]. Earth Science Frontiers, 24(6): 1−9 (in Chinese with English abstract).

Zhang A, Mo X, Yuan W, et al. 2017a. Petrogensis and tectonic setting of the Yemaquan granite from the iron−polymetallic ore area of Qimantag, Eastern Kunlun Mountains, Qinghai–Tibet Plateau[J]. Island Arc, 26(4): e12190.

Zhang J Y, Ma C Q, Xiong F H, et al. 2014. Early Paleozoic high−Mg diorite−granodiorite in the eastern Kunlun Orogen, western China: Response to continental collision and slab break−off[J]. Lithos, 210: 129−146.

Zhang L, Zhang H, Zhang S, et al. 2017b. Lithospheric delamination in post−collisional setting: evidence from intrusive magmatism from the North Qilian orogen to southern margin of the Alxa block, NW China[J]. Lithos, 288: 20−34.

Zhang A K, Liu G L, Feng C Y, et al. 2013. Geochemical Characteristics and Ore−Controlling Factors of the Hutouya Polymetallic Deposit, Qinghai Province[J]. Mineral Deposits, (1): 94−108 (in Chinese with English abstract).

Zhang A S, Xie G Q, Liu W Y, et al. 2023. Identification of the first intermediate−sulfidation epithermal gold deposit in the Timok Metallogenic zone of Serbia, Western Tethys: A case study of the Zlatno Brdo gold deposit[J]. Geotectonica et Metallogenia, 47(5): 1110−1123 (in Chinese with English abstract).

Zhang C Y, Zhao Y, Liu J, et al. 2019. Provenance analysis of the Maoniushan Formation in the North Qaidam basin and its tectonic significance[J]. Acta Geologica Sinica, 93(3): 712−723 (in Chinese with English abstract).

Zhang X, Li Z, Jia Q, et al. 2016. Geochronology, geochemistry, and geological significance of granite porphyry in the Hutouya polymetallic deposit, Qimantage area, Qinghai Province[J]. Journal of Jilin University (Earth Science Edition), 46(3): 749−765 (in Chinese with English abstract).

Zhang Y L, Ni J Y, Shen Y X, et al. 2018. Zircon U−Pb ages and geological significance of volcanic rocks from Maoniushan Formation in the northern margin of Qaidam Basin[J]. Geoscience, 32(2): 329−334 (in Chinese with English abstract).

Zhang Y, Zhang D M, Liu G Y, et al. 2017. M. Zircon U−Pb dating of porphyroid monzonitic granite in the Kaerqueka copper polymetallic deposit of East Kunlun Mountains and its geological significance[J]. Geological Bulletin of China, 36(2/3): 270−274 (in Chinese with English abstract).

Zhang Z W, Wang Y L, Qian B, et al. 2017. Zircon SHRIMP U−Pb age of the Binggounan magmatic Ni−Cu deposit in East Kunlun Mountains

and tectonic implications[J]. Acta Geologica Sinica, 91(4): 724−735 (in Chinese with English abstract).
Zhang Z Y, Sun F Y, Wang Q, et al. 2019. Zircon U−Pb chronology and geochemical characteristics of Late Devonian granite porphyry in the Mohexiala silver polymetallic deposit of Eastern Kunlun, Qinghai[J]. Global Geology, 38(2): 309−321 (in Chinese with English abstract).
Zhao C S, Yang F Q, Dai J Z. 2006. Metallogenic age of the Kendekeke Co, Bi, Au deposit in East Kunlun Mountains, Qinghai Province, and its significance[J]. Mineral Deposits, 25: 427−430 (in Chinese with English abstract).
Zhao S F, Wu Z S, Zhang A K, et al. 2014. Geological features, deposit genesis and prospecting potential of Changshan molybdenum deposit in Qimantage, Qinghai Province[J]. Northwestern Geology, 47(1): 179−187 (in Chinese with English abstract).
Zhao Z Y. 2019. Mineralogy and Mineralization of the Skarn at the Niukutou Deposit, Qinghai[D]. Master Thesis of China University of Geosciences (Beijing)(in Chinese with English abstract).
Zheng Z, Chen Y J, Deng X H, et al. 2018. Origin of the Bashierxi monzogranite, Qiman Tagh, East Kunlun Orogen, NW China: A magmatic response to the evolution of the Proto−Tethys Ocean[J]. Lithos, 296/299: 181−194.
Zheng Z, Chen Y J, Deng X H, et al. 2016. Muscovite $^{40}Ar/^{39}Ar$ dating of the Baiganhu W−Sn orefield, Qimantag, East Kunlun Mountains, and its geological implications[J]. Geology in China, 43(4): 1341−1352 (in Chinese with English abstract).
Zhong S, Feng C, Seltmann R, et al. 2018. Geochemical contrasts between Late Triassic ore−bearing and barren intrusions in the Weibao Cu–Pb–Zn deposit, East Kunlun Mountains, NW China: constraints from accessory minerals (zircon and apatite)[J]. Mineralium Deposita, 53: 855−870.
Zhong S, Li S, Feng C, et al. 2021a. Geochronology and geochemistry of mineralized and barren intrusive rocks in the Yemaquan polymetallic skarn deposit, northern Qinghai−Tibet Plateau: A zircon perspective[J]. Ore Geology Reviews: 139.
Zhong S, Li S, Feng C, et al. 2021b. Porphyry copper and skarn fertility of the northern Qinghai−Tibet Plateau collisional granitoids[J]. Earth−Science Reviews, 214: 103524.
Zhong S, Seltmann R, Qu H, et al. 2019. Characterization of the zircon Ce anomaly for estimation of oxidation state of magmas: a revised Ce/Ce* method[J]. Mineralogy and Petrology, 113: 755−763.
Zhong S H. 2018. Genesis of the Weibao Cu−Pb−Zn deposit in Xinjiang, China[D]. Doctoral Thesis of Chinese Academy of Geological Sciences (in Chinese with English abstract).
Zhou J, Feng C, Li D, et al. 2016. Geological, geochemical, and geochronological characteristics of Caledonian W–Sn mineralization in the Baiganhu orefield, southeastern Xinjiang, China[J]. Ore Geology Reviews, 75: 125−149.
Zhu J J, Hu R, Bi X W, et al. Porphyry Cu fertility of eastern Paleo−Tethyan arc magmas: Evidence from zircon and apatite compositions[J]. Lithos, 2022, 424: 106775.
Zhu R X, Zhao P, Zhao L. 2022. Evolution and Dynamical Processes of the New Tethys Ocean[J]. Scientia Sinica (Terrae), 52(1): 1–25 (in Chinese with English abstract).

附中文参考文献

白宜娜, 孙丰月, 钱烨, 等. 2016. 青海东昆仑尕林格铁多金属矿床辉石闪长岩 U−Pb 年代学及地球化学特征[J]. 世界地质, 35(1): 17−27.
陈博, 张占玉, 耿建珍, 等. 2012. 青海西部祁漫塔格山卡尔却卡铜多金属矿床似斑状黑云二长花岗岩 LA−ICP−MS 锆石 U−Pb 年龄[J]. 地质通报, 31(2/3): 463−468.
陈静, 胡继春, 逯永卓, 等. 2018. 东昆仑小灶火地区钼矿化正长花岗岩年代学、地球化学特征及其地质意义[J]. 黄金科学技术, 26(4): 465−472.
陈隽璐, 黎敦朋, 李新林, 等. 2024. 东昆仑祁漫塔格山南缘黑山蛇绿岩的发现及其特征[J]. 陕西地质, (2): 35−46.
丁林. 2024. 特提斯地球动力系统研究新进展 [J]. 中国科学: 地球科学, 54(3): 892−896.
杜立华, 黄宇, 高雄, 等. 2025. 内蒙古维拉斯托稀有金属-锡多金属矿床强还原性成矿斑岩特征及其对矿床成因的约束[J]. 地质通报, 44(4):633-648.
丰成友, 李东生, 屈文俊, 等. 2009. 青海祁漫塔格索拉吉尔矽卡岩型铜钼矿床辉钼矿铼-锇同位素定年及其地质意义[J]. 岩矿测试, 28(3): 223−227.
丰成友, 李东生, 吴正寿, 等. 2010. 东昆仑祁漫塔格成矿带矿床类型、时空分布及多金属成矿作用[J]. 西北地质, 43(4): 10−17.
丰成友, 王松, 李国臣, 等. 2012. 青海祁漫塔格中晚三叠世花岗岩: 年代学、地球化学及成矿意义[J]. 岩石学报, 28(2): 665−678.
丰成友, 王雪萍, 舒晓峰, 等. 2011. 青海祁漫塔格虎头崖铅锌多金属矿区年代学研究及地质意义[J]. 吉林大学学报 (地球科学版), 41(6): 1806−1817.
傅恒, 韩建辉, 孙煜新, 等. 2024. 特提斯造山带[J]. 沉积与特提斯地质, 44(1): 100−33.
高永宝, 李侃, 钱兵, 等. 2018. 东昆仑卡而却卡铜钼铁多金属矿床成矿年代学: 辉钼矿 Re−Os 和金云母 Ar−Ar 同位素定年约束[J]. 大地构造与成矿学, 42(1): 96−107.
高永宝, 李文渊, 李侃, 等. 2012. 东昆仑祁漫塔格白干湖-戛勒赛矿带成岩成矿时代及钨锡成矿作用[J]. 西北地质, 45(4): 229−241.
高永宝, 李文渊, 钱兵, 等. 2014. 东昆仑野马泉铁矿相关花岗质岩体年代学、地球化学及 Hf 同位素特征[J]. 岩石学报, 30(6): 1647−1665.
高永宝. 2013. 东昆仑祁漫塔格地区中酸性侵入岩浆活动与成矿作用[D]. 长安大学博士学位论文.
耿健. 2023. 青海牛苦头矿区两期岩浆岩与成矿研究[D]. 中国地质大学 (北京) 硕士学位论文.
顾焱, 钱烨, 李予晋, 等. 2019. 东昆仑骆驼峰地区中晚三叠世花岗岩年代学、地球化学及构造意义[J]. 矿产勘查, 10(4): 724−736.
郭广慧, 钟世华, 李三忠, 等. 2023. 运用机器学习和锆石微量元素构建花岗岩成矿潜力判别图解: 以东昆仑祁漫塔格为例[J]. 西北地质, 56(6): 57−70.
郭通珍, 刘荣, 陈发彬, 等. 2011. 青海祁漫塔格山乌兰乌珠尔斑状正长花岗岩 LA−MC−ICPMS 锆石 U−Pb 定年及地质意义[J]. 地质通报, 30(8): 1203−1211.
韩海臣, 王国良, 丁玉进, 等. 2018. 东昆仑巴音呼都森晚三叠世中酸性侵入岩锆石 LA−ICP−MSU−Pb 定年及地质意义[J]. 西北地质,

51(1): 144−158.
郝娜娜, 袁万明, 张爱奎, 等. 2014. 东昆仑祁漫塔格晚志留世—早泥盆世花岗岩: 年代学、地球化学及形成环境[J]. 地质论评, 60(1): 201−215.
何书跃, 白国龙, 刘智刚, 等. 2025. 青海省成矿规律初探[J]. 地质通报, 44(4): 649-678.
何书跃, 李东生, 白国龙, 等. 2018. 青海祁漫塔格群力矿床矽卡岩中白云母$^{40}Ar/^{39}Ar$年龄报道[J]. 中国地质, 45(1): 201−202.
何书跃, 李东生, 李良林, 等. 2009. 青海东昆仑鸭子沟斑岩型铜 (钼) 矿区辉钼矿铼-锇同位素年龄及地质意义[J]. 大地构造与成矿学, 33(2): 236−242.
何书跃, 林贵, 钟世华, 等. 2023. 造山作用孕育"青海金腰带"[J]. 西北地质, 56(6): 1−16.
侯增谦, 潘小菲, 杨志明, 等. 2007. 初论大陆环境斑岩铜矿[J]. 现代地质, (2): 332−351.
侯增谦. 2010. 大陆碰撞成矿论[J]. 地质学报, 84(1): 30−58.
黄宇, 钟世华, 李三忠, 等. 2025. 副矿物包裹体和信号采集时间对锆石 U−Pb 年龄和微量元素分析结果的影响[J]. 地学前缘, 32(1): 388−400.
孔会磊, 李金超, 黄军, 等. 2015. 东昆仑小圆山铁多金属矿区斜长花岗斑岩锆石 U−Pb 测年、岩石地球化学及找矿意义[J]. 中国地质, 42(3): 521−532.
孔会磊, 李金超, 栗亚芝, 等. 2016. 青海祁漫塔格小圆山铁多金属矿区英云闪长岩 LA−MC−ICP−MS 锆石 U−Pb 测年及其地质意义[J]. 地质科技情报, 35(1): 8−16.
寇贵存, 冯金炜, 罗保荣, 等. 2017. 青海阿木尼克山地区牦牛山组火山岩地球化学特征、锆石 U−Pb 年龄及其地质意义[J]. 地质通报, 36(2/3): 275−284.
李洪茂, 时友东, 刘忠, 等. 2006. 东昆仑山若羌地区白干湖钨锡矿床地质特征及成因[J]. 地质通报, (2/3): 277−281.
李洪普, 刘具仓, 张喜全, 等. 2011. 青海省柴南缘四角羊铁多金属矿区岩浆岩特征及其成矿意义[J]. 地质与勘探, 47(6): 1009−1017.
李积清, 陈静, 史青瑞, 等. 2016. 东昆仑卡尔却卡矿区似斑状二长花岗岩成因: 锆石 U−Pb 年龄及 Sr−Nd 同位素制约[J]. 矿物岩石, 36(3): 87−95.
李加多, 王新雨, 祝新友, 等. 2019. 青海祁漫塔格海西期成矿初探——以牛苦头 M1 铅锌矿床为例[J]. 矿产勘查, 10(8): 1775−1783.
李侃, 高永宝, 钱兵, 等. 2015. 东昆仑祁漫塔格虎头崖铅锌多金属矿区花岗岩年代学、地球化学及 Hf 同位素特征[J]. 中国地质, 42(3): 630−645.
李三忠, 赵淑娟, 李玺瑶, 等. 2016. 东亚原特提斯洋 (Ⅰ): 南北边界和俯冲极性[J]. 岩石学报, 32(9): 2609−2627.
李三忠, 赵淑娟, 余珊, 等. 2016. 东亚原特提斯洋 (Ⅱ): 早古生代微陆块亲缘性与聚合[J]. 岩石学报, 32(9): 2628−2644.
李世金, 孙丰月, 丰成友, 等. 2008. 青海东昆仑鸭子沟多金属矿的成矿年代学研究[J]. 地质学报, (7): 949−955.
李文渊. 2024. 古特提斯构造演化及其成矿作用[J]. 地质学报, 98(11): 3255−3273.
李忠海, 崔峰源, 杨舒婷, 等. 2023. 特提斯演化的关键动力学过程与驱动力[J]. 中国科学: 地球科学, 53(12): 2701−2722.
刘嘉情, 钟世华, 李三忠, 等. 2023. 基于机器学习和全岩成分识别东昆仑祁漫塔格斑岩-矽卡岩矿床成矿岩体和贫矿岩体[J]. 西北地质, 56(6): 41−56.
刘建楠, 2018. 青海野马泉铁锌矿床多期次构造岩浆热年代学成矿意义[D]. 中国地质科学院博士学位论文
陆济璞, 李江, 覃小锋, 等. 2005. 东昆仑祁漫塔格伊涅克阿干花岗岩特征及构造意义[J]. 沉积与特提斯地质, (4): 46−54.
刘云华, 莫宣学, 张雪亭, 等. 2006. 东昆仑野马泉地区矽卡岩矿床地球化学特征及其成因意义[J]. 华南地质与矿产, 3: 31−36.
吕鹏瑞, 姚文光, 张辉善, 等. 2020. 特提斯成矿域中新世斑岩铜矿岩石成因、源区、构造演化及其成矿作用过程[J]. 地质学报, 94(8): 2291−2310.
毛景文, 周振华, 丰成友, 等. 2012. 初论中国三叠纪大规模成矿作用及其动力学背景[J]. 中国地质, 39(6): 1437−1471.
乔保星, 潘彤, 陈静. 2016. 东昆仑野马泉铁多金属矿床花岗闪长岩年代学、地球化学特征及其地质意义[J]. 青海大学学报 (自然科学版), 34(1): 63−73.
瞿泓滢, 丰成友, 裴荣富, 等. 2015. 青海祁漫塔格虎头崖多金属矿区岩体热年代学研究[J]. 地质学报, 89(3): 498−509.
瞿泓滢, 刘建楠, 裴荣富, 等. 2018. 青海祁漫塔格成矿带与虎头崖铜铅锌多金属矿床有关的二长花岗岩体热年代学研究[J]. 中国地质, 45(3): 511−527.
佘宏全, 张德全, 景向阳, 等. 2007. 青海省乌兰乌珠尔斑岩铜矿床地质特征与成因[J]. 中国地质, (2): 306−314.
时超, 李荣社, 何世平, 等. 2017. 东昆仑祁漫塔格虎头崖铅锌多金属矿成矿时代及其地质意义——黑云二长花岗岩地球化学特征和锆石 U−Pb 年龄证据[J]. 地质通报, 36(6): 977−986.
宋泰忠, 赵海霞, 张维宽, 等. 2010. 祁漫塔格地区十字沟蛇绿岩地质特征[J]. 西北地质, 43(4): 124−133.
宋忠宝, 张雨莲, 贾群子, 等. 2014. 东昆仑祁漫塔格地区野马泉深部的华力西期花岗闪长岩 U−Pb 年龄及其意义[J]. 现代地质, 28(6): 1161−1169.
谈生祥, 郭通珍, 董进生, 等. 2011. 青海乌兰乌珠尔地区晚志留世过铝质花岗岩地质特征及意义[J]. 青海大学学报 (自然科学版), 29(1): 36−43.
唐菊兴, 多吉, 刘鸿飞, 等. 2012. 冈底斯成矿带东段矿床成矿系列及找矿突破的关键问题研究[J]. 地球学报, 33(4): 393−410.
唐菊兴. 2019. 青藏高原及邻区重要成矿带矿产资源基地调查与研究进展[J]. 岩石学报, 35(3): 617−624.
田承盛, 丰成友, 李军红, 等. 2013. 青海它温查汉铁多金属矿床$^{40}Ar-^{39}Ar$年代学研究及意义[J]. 矿床地质, 32(1): 169−176.
汪洋. 2017. 青海祁漫塔格虎头崖铜铁多金属矿床地质特征及矿化富集规律研究[D]. 吉林大学硕士学位论文.
王秉璋, 潘彤, 任海东, 等. 2021. 东昆仑祁漫塔格寒武纪岛弧: 来自拉陵高里河地区玻安岩型高镁安山岩/闪长岩锆石 U−Pb 年代学、地球化学和 Hf 同位素证据[J]. 地学前缘, 28(1): 318−333.
王富春, 陈静, 谢志勇, 等. 2013. 东昆仑拉陵灶火钼多金属矿床地质特征及辉钼矿 Re−Os 同位素定年[J]. 中国地质, 40(4): 1209−1217.
王冠, 孙丰月, 李碧乐, 等. 2014. 东昆仑夏日哈木铜镍矿镁铁质-超镁铁质岩体岩相学、锆石 U−Pb 年代学、地球化学及其构造意义[J]. 地学前缘, 21(6): 381−401.
王瑞, 朱弟成, 王青, 等. 2020. 特提斯造山带斑岩成矿作用[J]. 中国科

学: 地球科学, 50(12): 1919−1946.
王松, 丰成友, 李世金, 等. 2009. 青海祁漫塔格卡尔却卡铜多金属矿区花岗闪长岩锆石 SHRIMP U−Pb 测年及其地质意义[J]. 中国地质, 36(1): 74−84.
王新雨, 王书来, 吴锦荣, 等. 2023. 青海省牛苦头铅锌矿床成矿时代研究: 来自成矿岩体年代学和黄铁矿 Re–Os 地球化学证据[J]. 西北地质, 56(6): 71−81.
王新雨, 王书来, 刘明, 等. 2024. 青海省祁漫塔格牛苦头铅锌矿床年代学与矿物微量元素特征研究[J/OL]. 地学前缘: 1−27. https://doi.org/10.13745/j.esf.sf.2024.11.27.
王增振, 韩宝福, 丰成友, 等. 2014. 新疆白干湖地区花岗岩年代学、地球化学研究及其构造意义[J]. 岩石矿物学杂志, 33(4): 597−616.
吴福元, 万博, 赵亮, 等. 2020. 特提斯地球动力学[J]. 岩石学报, 36(6): 1627−1674.
吴祥珂, 孟繁聪, 许虹, 等. 2011. 青海祁漫塔格玛兴大坂晚三叠世花岗岩年代学、地球化学及 Nd−Hf 同位素组成[J]. 岩石学报, 27(11): 3380−3394.
吴宗昌. 2017. 东昆仑造山带拉陵灶火中游博武斑岩钼矿成因与找矿潜力[D]. 中国地质大学 (北京) 硕士学位论文.
奚仁刚, 校培喜, 伍跃中, 等. 2010. 东昆仑肯德可克铁矿区二长花岗岩组成、年龄及地质意义[J]. 西北地质, 43(4): 195−202.
肖晔, 丰成友, 刘建楠, 等. 2013. 青海肯德可克铁多金属矿区年代学及硫同位素特征[J]. 矿床地质, 32(1): 177−186.
辛仁臣. 2024. 全球特提斯构造域及其时空分布[J/OL]. 沉积与特提斯地质, 1−20. https://doi.org/10.19826/j.cnki.1009-3850.2024.10002.
许庆林, 2014. 青海东昆仑造山带斑岩型矿床成矿作用研究[D]. 吉林大学博士学位论文.
薛宁, 安勇胜, 李五福, 等. 2009. 青海野马泉地区正长花岗岩的基本特征及成因[J]. 青海大学学报 (自然科学版), 27(2): 18−22.
严玉峰, 杨雪松, 陈发彬, 等. 2012. 东昆仑-拉陵灶火中游含钼花岗岩的特征[J]. 中国科技信息, (18): 37−39.
杨金中, 沈远超, 李光明, 等. 1999. 新疆东昆仑鸭子泉蛇绿岩的基本特征及其大地构造意义[J]. 现代地质, (3): 309−314.
杨涛, 李智明, 张乐, 等. 2017. 东昆仑它温查汉西花岗岩地质地球化学特征及其构造意义[J]. 高校地质学报, 23(3): 452−464.
姚磊, 吕志成, 赵财胜, 等. 2016. 青海祁漫塔格地区牛苦头矿床和卡而却卡矿床 B 区花岗质岩石 LA−ICP−MS 锆石 U−Pb 年龄——对泥盆纪成岩成矿作用的指示[J]. 地质通报, 35(7): 1158−1169.
姚磊. 2015. 青海祁漫塔格地区三叠纪成岩成矿作用及地球动力学背景[D]. 中国地质大学 (北京) 博士学位论文.
于淼. 2017. 青海祁漫塔格尕林格矽卡岩铁多金属矿成矿机理研究[D]. 中国地质大学 (北京) 博士学位论文.
于淼, 丰成友, 刘洪川, 等. 2015. 青海尕林格矽卡岩型铁矿金云母$^{40}Ar/^{39}Ar$年代学及成矿地质意义[J]. 地质学报, 89(3): 510−521.
于淼, 丰成友, 何书跃, 等. 2017. 祁漫塔格造山带——青藏高原北部地壳演化窥探[J]. 地质学报, 91(4): 703−723.
袁万明, 莫宣学, 张爱奎, 等. 2017. 青海省东昆仑斑岩带新发现[J]. 地学前缘, 24(6): 1−9.
张爱奎, 刘光莲, 丰成友, 等. 2013. 青海虎头崖多金属矿床地球化学特征及成矿-控矿因素研究[J]. 矿床地质, 32(1): 94−108.
张安顺, 谢桂青, 刘文元, 等. 2023. 特提斯成矿域西部塞尔维亚 Timok 矿集区首例中硫化型浅成低温金矿床的厘定: 以 Zlatno Brdo 金矿床为例[J]. 大地构造与成矿学, 47(5): 1110−1123.
张斌武. 2022. 青海祁漫塔格虎头崖铁铜铅锌多金属矿床磷灰石特征及其地质意义[D]. 中南大学硕士学位论文.
张春宇, 赵越, 刘金, 等. 2019. 柴达木盆地北缘牦牛山组物源分析及其构造意义[J]. 地质学报, 93(3): 712−723.
张雷. 2013. 东昆仑野马泉地区三叠纪构造岩浆作用与成矿关系[D]. 中国地质大学 (北京) 博士学位论文.
张晓飞, 李智明, 贾群子, 等. 2016. 青海祁漫塔格虎头崖多金属矿区花岗斑岩地球化学、年代学特征及其地质意义[J]. 吉林大学学报 (地球科学版), 46(3): 749−765.
张耀玲, 倪晋宇, 沈燕绪, 等. 2018. 柴北缘牦牛山组火山岩锆石 U−Pb 年龄及其地质意义[J]. 现代地质, 32(2): 329−334.
张勇, 张大明, 刘国燕, 等. 2017. 东昆仑卡而却卡铜多金属矿床似斑状二长花岗岩锆石 U−Pb 年龄及其地质意义[J]. 地质通报, 36(Z1): 270−274.
赵财胜, 杨富全, 代军治. 2006. 青海东昆仑肯德可克钴铋金矿床成矿年龄及意义[J]. 矿床地质, 25(S1): 427−430.
赵淑芳, 吴正寿, 张爱奎, 等. 2014. 青海祁漫塔格长山钼矿地质特征、矿床成因及找矿前景[J]. 西北地质, 47(1): 179−187.
赵子烨. 2019. 青海牛苦头矿床矽卡岩矿物学及成矿作用研究[D]. 中国地质大学 (北京) 硕士学位论文.
郑震, 陈衍景, 邓小华, 等. 2016. 东昆仑祁漫塔格地区白干湖钨锡矿田白云母$^{40}Ar/^{39}Ar$定年及地质意义[J]. 中国地质, 43(4): 1341−1352.
钟世华. 2018. 新疆维宝铜铅锌矿床成因研究[D]. 中国地质科学院博士学位论文.
朱日祥, 赵盼, 赵亮. 2022. 新特提斯洋演化与动力过程[J]. 中国科学: 地球科学, 52(1): 1−25.